Clays and Clay Minerals, Vol. 57, No. 5, 531–554, 2009.

PARTIAL DISSOLUTION OF GLAUCONITIC SAMPLES: IMPLICATIONS FOR THE METHODOLOGY OF K-Ar AND Rb-Sr DATING

ARKADIUSZ DERKOWSKI[1,*], JAN ŚRODOŃ[1], WOJCIECH FRANUS[2], PETER UHLÍK[3], MICHAŁ BANAŚ[1], GRZEGORZ ZIELIŃSKI[1], MARIA ČAPLOVIČOVÁ[3], AND MAŁGORZATA FRANUS[2]

[1] Institute of Geological Sciences, Polish Academy of Sciences, Senacka 1, 31-002 Kraków, Poland
[2] Department of Geotechnics, Lublin University of Technology, Nadbystrzycka 40, 20-618 Lublin, Poland
[3] Department of Geology of Mineral Deposits, Comenius University, Mlynská dolina, 842 15, Bratislava, Slovakia

Abstract—The K-Ar dating of glauconite has been used as an important stratigraphic tool for many decades. The application of this technique is limited to pure glauconites, free of detrital contamination by K-bearing phases, often not easy to detect. This study extends the application of isotope dating to the contaminated glauconites and offers a precise technique for detecting the detrital contamination of glauconites.

The most common K-bearing detrital contaminants have smaller (K-feldspars, Al-rich dioctahedral micas) or greater (trioctahedral micas) dissolution rates than glauconite in extremely low pH solutions. The differences in the dissolution rates can be applied to evaluate the purity of the glauconite and its crystallization age.

The interlaboratory GLO glauconite standard and grain-size fractions separated from glauconitic sandstones of the Paleogene (sample GL) and Jurassic (sample GW8) ages were treated with acid (3 M HCl, at 99±2ºC) for different reaction times (0.5−7 h) and measured for their apparent isotopic ages.

Microporous amorphous silica with large specific surface area is the solid product of the reaction and its content increases with reaction time. The K-Ar dates (apparent ages) of the solid residues increase significantly with reaction time: from 44.6 to 107 Ma for the GL sample and from 125.7 to 394.7 Ma for GW8. The increase is negligible in the case of the GLO standard. The Rb-Sr data of the GL sample were modeled using initial $^{87}Sr/^{86}Sr$ ratios of 0.707−0.709, which resulted in a 29.9−35.8 Ma date for the untreated portions of GL, and ~42.6 Ma after 7 h of treatment.

The increase of isotopic K-Ar date with increasing time of dissolution is interpreted to be a result of increasing concentration of detrital, acid-resistant, K-bearing minerals, observed also with the electron microscope and X-ray diffraction. Probabilistic modeling based on single (K-Ar) or double (K-Ar and Rb-Sr) isotopic systems evaluated the isotopic ages of the detrital and authigenic minerals, and their K_2O and Rb concentrations. The crystallization ages computed using these two methods are: 24.0, 26.5, and 32.3 Ma for the GL material, and 117.3−121.8 Ma for the GW8 series.

The proposed method based on partial dissolution is a potential tool for evaluating the reliability of glauconite dating.

Key Words—Acid Dissolution, Authigenic Minerals, Detrital Minerals, Glauconite, GLO, K-Ar Dating, Mixed Ages, Rb-Sr Dating.

INTRODUCTION

Since Evernden *et al*. (1961) identified glauconite as being a useful mineral for K-Ar dating, it has been utilized in geochronology. Glauconite is a ubiquitous K-bearing clay mineral that crystallizes syndepositionally in host sediments. Other K-minerals in sedimentary rocks are either detrital, diagenetic, rare (*e.g.* sedimentary neoformed K-feldspar, Sandler *et al*., 2004), or their K-Ar dating is difficult, *e.g.* halides (Brookins *et al*., 1980). Glauconite crystallizes on the sea floor, between 50 m and 300 m depth, often during transgression. It is very resistant to burial diagenesis, most often surviving without loss or gain of K and Ar. For these reasons it is useful for dating sedimentary processes (Odin, 1988), provided that it is not contaminated by detrital K-bearing phases.

Odin and Matter (1981) suggested that glauconitization starts on various granular substrates. During the first stage, a glauconitic Fe-rich smectite appears which recrystallizes into more micaceous particles (glauconite *s.s.*). During maturation on the seafloor, the substrate material 'disappears' and the K_2O content increases. Odin (1982) and Odin and Dodson (1982) suggested that 'evolved glauconite' (7−8% K_2O) is sufficiently well recrystallized to produce reliable K-Ar ages, because no evidence of the presence of precursor minerals can be found in such materials by X-ray diffraction (XRD).

The assumption that all the detrital components are dissolved or recrystallized during the glauconitization process may not be true in all cases. If the particles of detrital mica are enclosed within the evolved glauconitic grains, such mica may be non-separable using the

* E-mail address of corresponding author:
ndderkow@cyf-kr.edu.pl
DOI: 10.1346/CCMN.2009.0570503

standard methods of glauconite purification (Odin, 1969). In such a case the 'Odin conditions' are fulfilled (K_2O content, XRD characteristics, *etc.*) but the isotopic K-Ar age may be significantly greater. Simple modeling reveals that 4.4 wt.% of a Caledonian mica (K_2O = 9.5 wt.%; age 500 Ma) in highly evolved Eocene (50 Ma) glauconite (K_2O = 8.5 wt.%) raises the K-Ar age value to 75 Ma (Late Cretaceous). Such an error (50%) can result from a detrital contamination which is too small to be detectable by XRD or other standard methods because of the structural similarity of glauconite and other micas. Besides the amount of the detrital phase, the error also depends on the age difference between the glauconite and the contaminating material.

An opposite effect to the detrital K-bearing mineral contamination has also been observed during K-Ar dating of glauconite: dates measured are younger than the estimated sedimentary ages. Very sophisticated interpretations can be found in the literature (*e.g.* Kelley, 2002): spontaneous Ar recoil, diagenetic effect (illitization of smectitic glauconite layers), Ar loss from the edges of glauconite particles, or a long glauconitization process occurring under the sediment surface which can last millions of years after deposition. Based on the surface properties of glauconite, one can find much simpler explanations that should be excluded before any advanced interpretation. Glauconite crystallizes in marine environments, at the water-sediment interface, rich in the K necessary for the formation of mica. As a result one would expect K to occupy a significant proportion of all the exchangeable sites of glauconite. The radiogenic argon produced by that fraction of K is lost from the structure due to dramatically reduced Ar retention on the expandable (or external) surfaces, compared to Ar atoms trapped within the micaceous interlayer. Thus, many glauconites in the natural state are likely to show excess K coming from the adsorbed K. The effect of the excess K is presented in Figure 1, using the model of 40 Ma old glauconite, yielding the non-exchangeable K_2O content of 7.2%. An average cation exchange value (CEC) value of 15 meq/100 g was accepted after Manghnani and Hower (1964). The decreasing K-Ar date and increasing K_2O are shown as functions of percent exchangeable sites occupied by K. At full K-saturation the apparent age drops to 36.5 Ma, while total K_2O increases to 7.9%. This simulation indicates that a saturation with other cations (*e.g.* Ca, Na; details in Jackson, 1969) should always be an essential step of glauconite pretreatment before K-Ar dating. The effect described above does not disprove any concept of K-Ar dates of glauconite being too young; it merely warns about the trap to be avoided before any advanced interpretation of the glauconite is attempted.

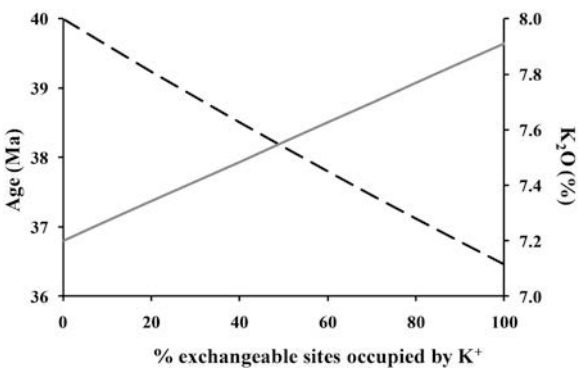

Figure 1. Simulation of the apparent K/Ar isotopic age (dashed black line) and total K_2O concentration (solid gray line) in glauconite (40 Ma old, structural K_2O = 7.2%, CEC = 15 meq/100 g) as functions of % exchangeable sites occupied by K^+ cations.

While the correction for adsorbed K requires only the cation exchange procedure, the detrital contamination remains a difficult challenge. To solve this problem one should remove one of the K-bearing materials. This can be attempted by taking advantage of the difference in the dissolution rates of various micaceous minerals. Acid treatment is a well-known technique, commonly used for clay-surface activation (*e.g.* Madejová *et al.*, 1998; Espantaleón *et al.*, 2003). The acid dissolution of phyllosilicates has been found to proceed incongruently and to cause reorganization of the tetrahedral sheet and its alteration to microporous silica (Madejová *et al.*, 1998; Temuujin *et al.*, 2003; Hassan and Baioumy, 2006). The dissolution rates of smectites in hydrochloric acid correlate positively with their Fe and Mg contents (Novák and Číčel, 1978), so we may expect a similar relationship for micas.

The dioctahedral Al-rich micas are less reactive than trioctahedral, so they are more likey to occur as detrital components in glauconitic grains. The kinetics of K dissolution from glauconite have been well described and modeled (Yadav *et al.*, 2000). Differences in the resistance against the acid attack show that glauconite is less stable than Al-micas but significantly more stable than trioctahedral micas (Kalinowski and Schweda, 1996; Józefaciuk and Bowanko, 2002). Thus, one can use acid treatment for partial separation of glauconite from its dioctahedral and trioctahedral impurities.

The acid-dissolution treatments of illite/smectite (Aronson and Douthitt, 1986) and glauconite (Thompson and Hower, 1973) have been applied to aid K-Ar dating, as have various treatments before Rb-Sr dating (Morton and Long, 1980, 1984), but those authors did not consider their results to be the consequences of the mineral heterogeneity of the investigated sample. K-Ar dates given by Aronson and Douthitt (1986), after progressive acid dissolution, did not reveal a coherent trend. Clauer *et al.* (1993) treated diagenetic Fe-rich illite with various reagents, including acids. After reaction under mild conditions (15 min at room temperature, 1 M HCl), which did not leach much of the Fe, they detected no significant changes in either

https://doi.org/10.1346/CCMN.2009.0570503 Published online by Cambridge University Press

K-Ar or Rb-Sr dates, but did find a decrease in Sr content (as described by Morton and Long, 1980), interpreted as due to the removal of a non-silicate component.

Assuming the coherent leaching of K, Rb, ^{40}Ar, and ^{87}Sr from the dissolved mineral, dating of pure, homogenous glauconite after subsequent dissolution steps should yield very close isotopic ages. In the present study, samples of glauconitic grains were tested, untreated and after partial dissolution in hydrochloric acid. The purpose of the present study was to investigate the homogeneity/heterogeneity of K-Ar and Rb-Sr systems of the glauconitic grains and to estimate the isotopic age of crystallization of glauconite in Cretaceous and Tertiary rocks, using the balanced 'differential calculation' of K-Ar and Rb-Sr data (modified approach of Chaudhuri *et al*., 1999) and probabilistic models.

MATERIALS AND METHODS

Samples

The interlaboratory glauconite GLO standard (Odin, 1982), used in this study as the reference material, is considered to be a perfectly homogenous, datable material (Odin, 1982). Two other samples were also investigated. Sample GL was separated from a glauconite-rich rock, collected from slightly compacted quartz sands in the Nowodwór quarry of Lubartów area (Lublin Upland, southeastern Poland). The sample was collected from one of the most glauconite-rich layers, from the center of a drilling core, recovered from a 10 m deep well, drilled in the glauconitic sand. The well did not reach the bottom of the glauconitic bed. The thickness of the glauconitic sand and the occasional occurrence of phosphate minerals suggest *in situ* crystallization rather than redeposition of the glauconite. Throughout the Lubartów area, these glauconite-bearing quartz sands overlie the Upper Eocene glauconitic sandstones, clays, and mudstones with phosphorites. They are covered by freshwater sands, of uncertain Miocene age (Gazda and Karaś, 2002), or a Pleistocene till (Uberna and Odrzywolska-Bieńkowa, 1977). The glauconite-bearing quartz sands are 12–30 m thick and poor in carbonate, which distinguishes them from the underlying marly Upper Eocene glauconitic sandstones (Łozińska-Stępień *et al*., 1985). Although no paleontologic record is available, if the glauconite is autochthonous then one might expect it to have crystallized between the Late Eocene and the end of the Miocene (~40–5 Ma, Gradstein *et al.*, 2004).

The GW8 glauconite was separated from the glauconite-bearing siltstone sample collected from the uppermost bed of the Wąwał section (Tomaszów Syncline, Central Poland; Łącka *et al.* 1989). The bed occurs above the Lower Hauterivian mudstones, which overlie the zone rich in the ammonite *Didochotomites bidichotomus (Leym.)* (Witkowski, 1967; Kaim, 2002), but underneath the Biała Góra series, dated for the Middle and Upper Albian (Marcinowski and Rudowski, 1980). Based on these stratigraphic constraints, the sedimentary age of the glauconitic siltstone ranges from ~135 to 100 Ma (Gradstein *et al.*, 2004).

Experimental methods

The glaucony was separated from the glauconitic rocks by washing, ultrasonic treatment, sieving in water suspension (63 μm sieve), drying at 60ºC, magnetic separation, and handpicking to produce purified concentrates. The glauconitic sample from the Lublin sandstone, prepared in the manner described, and exchanged to Ca-form (see below), without further treatment, was labeled GL Nat. An additional sieving was used for the glauconitic sample GW8 (Wąwał section) to produce the 0.3–0.6 mm fraction, which, in Ca-form without additional treatments, was labeled GW8 Nat.

Separate portions of samples GLO, GL, and GW8 were treated with 10% HCl solution at 99±2ºC, in a water bath, for 0.5 to 7 h. The solid reaction products were identified by the general sample name and the number of hours of reaction (*e.g.* GL 7h, GLO 0.5h). The initial solid/liquid ratio was 100 mg/mL for the sample GL and 33 mg/mL for the samples GLO and GW8. After the reaction, the residual solids were filtered, washed with deionized water, dried at 60ºC, and weighed after cooling. The <63 μm fraction, obtained after the separation of the GL Nat sample, was also treated with acid for 7 h, under the same conditions as the portions of the GL sample, to produce the residual solid labeled F 7h. No grinding or milling was used at any stage of the separation and treatment.

Both raw and treated portions of samples were analyzed for their mineral composition by XRD using an X'TRA Thermo ARL diffractometer, using side-loaded randomly oriented preparations. They were also investigated by field emission scanning electron microscopy in backscattered (BSE) and secondary electron (SEM) modes with an energy dispersive system (EDS), and by Fourier-transform infrared spectroscopy (FTIR) in the 400–3800 cm^{-1} range, using a Bio-Rad FTS-60 instrument and the KBr pelleting method (1 mg of glauconitic material mixed with 300 mg of dried KBr). Atomic absorption spectrophotometry (AAS, Philips PU 9100X), was used to determine Fe in the post-reaction solutions of the GW8 series, while in the GL solids the concentrations of Fe, Mg, and Al were measured by AAS after conventional dissolution in acids. The concentration of SiO_2 was determined by the conventional gravimetric method based on fusion with Na_2CO_3 prior to dissolution and silica precipitation in HCl, followed by silica evaporation by reaction with HF (modified after Olsen, 1910). The XRD and FTIR analyses required grinding of the sample material.

https://doi.org/10.1346/CCMN.2009.0570503 Published online by Cambridge University Press

For transmission electron microscopy (TEM) and high-resolution TEM (HRTEM) the materials were prepared by the embedding procedure of Tessier (1984). Natural (GL Nat) and treated (GL 3h and GL 7h) grains were coated with agar, saturated first with water and then with methanol and propylene oxide to expel all water, and then they were impregnated with Spurr's resin. Ultrathin sections, 70−90 nm thick, were cut by a Reichert Ultracut microtome using a diamond knife. The HRTEM images were obtained using a JEOL JEM-2000 FX electron microscope at 160 kV, with 60000× magnification, with underfocused conditions, using an objective aperture of 50 μm. The images were observed through a binocular with 10−40× magnification.

K-Ar dating was performed at the Institute of Geological Sciences, Polish Academy of Sciences in Kraków, following the procedure described in detail by Środoń *et al.* (2006). Each portion was split into two aliquots: ~100 mg for K determination and ~50 mg for Ar isotopic analysis. Potassium was determined by flame emission spectrophotometry (Sherwood Model 420). During K measurement, the international standards NIST 70a and NIST 76a were used as external standards. Argon was released and purified by an extraction method similar to that described by Bonhomme *et al.* (1975). The method involves addition of ^{38}Ar spike and correction for atmospheric ^{40}Ar (^{36}Ar/^{40}Ar = 295.5). The fraction of ^{40}Ar* in total ^{40}Ar is labeled as %^{40}Ar*. The samples were fused in Mo-Ta crucibles in a resistance furnace, and the released gas was purified using a cold-trap and Ti and Al-Zr getters. The analytical precision was evaluated by periodic measurement of the international standard GLO. The mean of six determinations made previously is $24.99\pm0.20\times10^{-6}$ cm^3/g STP (1115.6±8.93 pmol/g), while the accepted value is $24.85\pm0.48\times10^{-6}$ cm^3/g STP (1109.4±21.43 pmol/g; Odin, 1982). The accepted concentration of K in GLO is 6.56±0.06 wt.% (Odin, 1982), while the measured K_2O concentration is 7.90±0.04 wt.% (6.56±0.03 wt.%). The repeatability of the GLO glauconite K-Ar dates that are calculated with the decay constants recommended by Steiger and Jaeger (1977) is better than ±2%. Because HCl was used in the partial dissolution procedure, the ^{35}Cl and ^{37}Cl isotopes of the residual chlorine (if remaining after washing and dialysis) might have been expected to interfere with the mass spectrometer measurement of Ar isotopes, due to the mass similarity. The mass spectrometer resolution was checked and found to allow measurement of the Cl and Ar isotope peaks separately.

All materials used for the K-Ar dating were exchanged into Ca-form (Jackson, 1969) before the analytical work began, to remove all K from exchangeable positions where it might have been trapped during dissolution.

The Rb-Sr methodology of Bachliński and Smulikowski (2002) was applied. Portions of the untreated material and of the solid residues from the acid treatment (no cation exchange procedure was applied) were dissolved in HNO_3+HF+HCl solution, and Sr and Rb were separated on chromatographic columns filled with AG 50W-X8 resin (Bio-Rad Laboratories, USA). Rb and Sr concentrations were determined by the isotope dilution method using ^{87}Rb (50.4 ppm) + ^{84}Sr (0.8 ppm) mixed spike. The isotope ratios were measured using a TIMS VG Sector 54 mass spectrometer in multi-collector dynamic mode at the Institute of Geological Sciences, Polish Academy of Sciences in Warsaw. The value of ^{86}Sr/^{88}Sr = 0.1194 was used to correct for the ion-beam fractionation. During Sr isotope analysis, the NIST SRM 987 standard was measured repeatedly, yielding an average ratio of ^{87}Sr/^{86}Sr = 0.710252±0.000011 (n = 77). No measured ^{87}Sr/^{86}Sr isotopic ratio exceeded the 0.004% error limit. The concentrations of Rb and Sr were calculated from the measured isotope ratios. The ^{87}Rb/^{86}Sr measurement error is considered to be 1%.

The cation exchange capacity (CEC) was determined by the method of Orsini and Remy (1976), employing Co(III) hexamine chloride. The method relies on the spectrometric measurement of the Co hexamine content in solution using the 470 nm wavelength. The absorbance is inversely related to the amount of $[Co(NH_3)_6]^{3+}$ cation adsorbed by 0.5−1 g of the tested material after it has been mixed with 25 mL of the Co(III) hexamine chloride solution.

The surface area (SA) was calculated from the adsorption and desorption isotherms of argon, measured at 77.5 K, using the monolayer gas adsorption theory of Brunauer, Emmett, and Teller (BET; Gregg and Sing, 1982).

Probabilistic model

Using a non-linear optimization engine from the *Premium Solver Platform*™ 8.0 (Frontline Systems Co. (Incline Village, Nevada, USA), a probabilistic calculation model was built in a *MS Excel*™ spreadsheet. The model assumes that the studied sample is a mixture of an authigenic glauconite and one detrital phase bearing Rb and K, plus some contamination devoid of these elements. Even if more than one K-bearing impurity is present, simplifying the model and reducing the number of degrees of freedom are necessary. The Rb/K ratio in the glauconite may be much greater than in the detrital mineral. The crystallization ages of both the glauconite and the detrital mineral are assumed to be the same for the Rb-Sr and K-Ar system, although in nature they may show slightly different closure times due to different properties of Sr and Ar atoms. The fraction of the detrital mineral in a solid portion tested must be the same for the Rb-Sr and K-Ar systems. Even though K and Rb concentrations of the glauconite may decrease due to reduction of the crystal thickness, one average concentration is assumed for all the solid portions.

The ranges of amorphous silica content are estimated based on the decrease in K_2O with respect to the untreated portions (no amorphous silica), and on quartz content from the SEM images and the XRD patterns. The results were optimized based on the mean concentrations (MIX) of Rb and K_2O weighted by the wt.% of three components of a given portion of the sample: glauconite (GLAUC), detrital mica+K-feldspar (DETR), and amorphous silica plus quartz and pyrite that are inactive in these isotopic systems (INACT):

$$K_2O_{MIX} = \frac{K_2O_{GLAUC} \times \%GLAUC + K_2O_{DETR} \times \%DETR}{100} \times \left(1 - \frac{\%INACT}{100}\right) \quad (1)$$

The calculation for Rb is analogous. The K and Rb concentrations and the K-Ar and Rb-Sr isotopic ages are the optimized values for glauconite and the detrital mineral. The concentrations of ^{87}Sr and $^{40}Ar^*$ were calculated from the isotopic ages and ^{87}Rb and K_2O, respectively. All these values were fitted simultaneously for all portions of the glauconitic material. In the same fitting run the fraction of the glauconite (GLAUC) and the isotopically inactive impurity (INACT) were optimized for each portion. The calculated values for each portion were compared to the measured values of K_2O and Rb concentrations, K-Ar and Rb-Sr isotopic ages, and the Rb/K ratio (parameters). The total error was taken as the minimization target for the model. All details of the probabilistic calculations are given in the Appendix.

RESULTS

Mineralogical and chemical changes during the dissolution of glauconite

Quantitative XRD analysis (Środoń *et al.*, 2001) using QUANTA software (proprietary of Chevron Energy Technology Co., Houston, Texas) revealed the following mineral composition of the bulk glauconitic sand from the Lublin area (the parent rock of GL sample): glauconite 60%, dioctahedral smectite 8.2%, dioctahedral Al-mica ($2M_1$ polytype) 7%, quartz 19%, and traces of kaolinite and K-feldspar (~2% each). Match: 99.96%. The sample collected in the Wąwał section (the parent rock of the GW8 sample) is a clayey siltstone with shell debris consisting of quartz and glauconite, with illite, beidellite, kaolinite, and carbonates, the last being represented mainly by calcite and siderite (Łącka *et al*., 1989).

The natural glauconitic material from Lublin area (GL Nat) is an almost pure micaceous phase that belongs to the 1*M* polytype (Figure 2a). The XRD pattern displays well developed 112 and $11\bar{2}$ reflections (peaks at 3.66 Å and 3.10 Å), characteristic of the 1*M* polytype, and a very sharp 001 reflection at 10.07 Å, typical of micas. Traces of quartz can be detected in the untreated glauconitic grains (Figures 2a, 3) which are mineralized microfossils (Figure 3). Glauconite GW8 represents a less mature and less structurally ordered phase (Figure 4), with a greater smectitic component (glauconite-nontronite) than GL, as shown by the broad 001 reflection at 11.2 Å. The GW8 glauconite is a mixture of polytypes 1*Md* and 1*M*. Traces of quartz, pyrite, and mica were observed within the untreated glauconitic grain (Figure 5, mica identification confirmed by EDS).

According to Odin's classification (Odin and Matter, 1981), both glauconitic materials can be considered as evolved, datable glauconite (authigenic shapes of grains, no traces of reworking or redeposition); the variability in maturation is obvious, however. The ordered structure and the K_2O content of GL (7.28%) makes it close to the highly evolved type (K_2O > 8%), while GW8 (6.25% K_2O) stays on the boundary of a little-evolved glauconite (K_2O 4–6%). Such a classification, based on the K_2O content, is consistent with their structural characteristics (Amorosi, 1997). The standard GLO glauconite is the most evolved of the materials studied: it contains 7.9% K_2O (value averaged from several analyses).

The diffraction patterns of the untreated glauconite portions (GL Nat – Figure 2a and GW8 Nat – Figure 4) do not reveal any non-coincident peaks of Al-rich dioctahedral 2:1 clay or feldspar. A weak band at ~1.50 Å, *i.e.* at the position of the 060 peak of Al-dioctahedral clay (Figure 2a), may represent glauconite (reflection 330: Brindley and Brown, 1980, p. 63).

The glauconitic material lost mass in the course of the acid treatment (Table 1, column 2). During subsequent steps of dissolution, the glauconite content was reduced while its structure remained unchanged. The increase in background in the 15–35º2θ range (Figures 2a, 4) was caused by an increase in the amount of X-ray amorphous silica. Traces of quartz became more noticeable after several hours of reaction, because of the decreasing glauconite content. The position of the 060 reflection (1.516–1.517 Å) did not shift, but extended dissolution of the GL sample made the peak at ~1.50 Å (characteristic position of Al-rich dioctahedral micas) greater than the 1.517 Å peak (Figure 2a). The XRD pattern of the material left after the complete dissolution of GW8 glauconite revealed, besides quartz content, a very small peak at 1.503 Å (Figure 4), indicating increasing contents of discrete Al-dioctahedral clay. The relative increase of Al-dioctahedral clay and probably other detrital minerals in both glauconitic samples in the course of dissolution is supported by the mineral composition of the <63 μm fraction after 7 h of acid treatment (F 7h). In addition to micas (Al-rich and glauconite) and quartz, this residual solid contained kaolinite and K-feldspar (Figure 2b).

The acid treatment had little effect on the grain morphology (Figure 3). BSE imaging and EDS linescans showed that the dissolution follows cracks and depletes the glauconitic grains of the octahedral and interlayer

https://doi.org/10.1346/CCMN.2009.0570503 Published online by Cambridge University Press

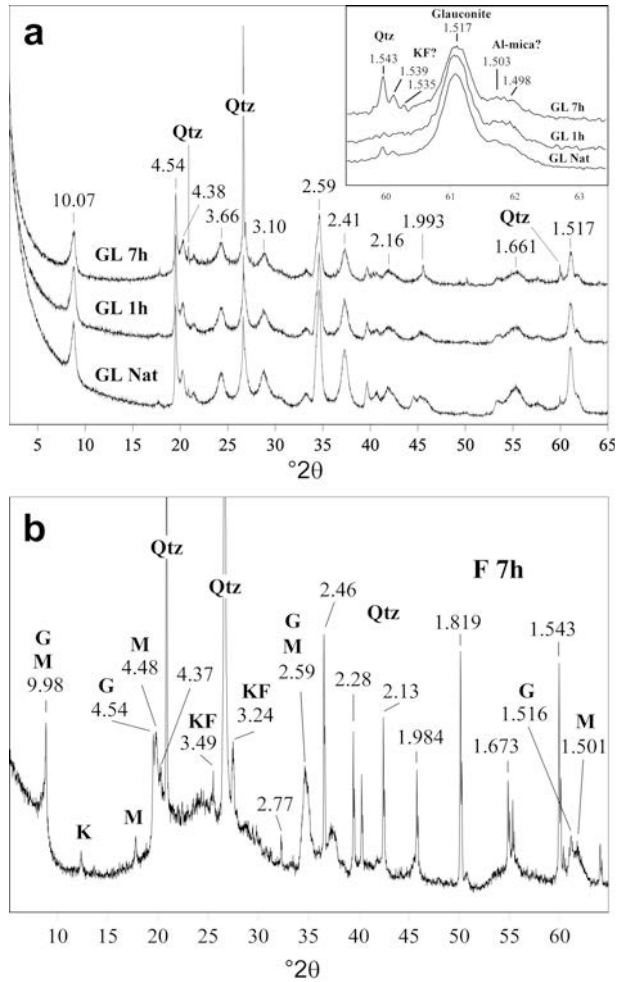

Figure 2. (a) XRD patterns of random preparations of glauconitic grains from the series GL, natural and after dissolution reaction (1 and 7 h). Upper right: zoom of the 060 range. (b) XRD pattern of the random preparation of the <63 μm fraction (sample GL) treated with acid for 7 h (F 7h). The raised background at 15–30°2θ represents amorphous silica. Qtz – quartz; KF – K-feldspar; M – Al-mica; G – glauconite.

elements (Figure 3). The strongest depletion in the dissolution zones was for Fe and Mg and less for K and Al. These zones are significantly enriched in silicon, up to almost 100% SiO_2, with a trace amount of Al. Acid treatment, which decreases K, Fe, and Mg in glauconitic grains, made the insoluble phases more distinguishable in BSE images. In the untreated portion of GW8, the barely noticeable mica revealed chemical characteristics very different from the surrounding glauconitic material: greater K and smaller Fe concentrations (Figure 5). After 1 h of dissolution, the mica particle remained less altered than the glauconitic material. The occurrence of unaltered Al-rich mica remained consistent with the XRD characteristics of the 060 region (Figure 4).

The glauconitic grains of sample GL consisted of crystals varying in thickness from 2 to ~30 nm (Figure 6). The crystal thickness distribution of natural glauconite (Figure 7) did not have an ideal lognormal shape, which is characteristic of illite (Środoń *et al*., 2000). The zigzag shape was probably due to imprecise statistics (Uhlík *et. al.*, 2000; Dudek *et al*., 2002) and the occurrence of micaceous minerals with a crystal thickness distribution different from the glauconite studied. The dissolution caused a noticeable decrease in the mean crystal thickness and a substantial change of the thickness distribution shape after only 7 h of treatment (Figure 7). The HRTEM observations also documented the formation of an amorphous phase after 7 h of dissolution (Figure 6c).

Significant decreases in the relative amounts of interlayer and octahedral cations and of the CEC were observed, while the external surface area (SA-BET; the gas adsorption procedure does not measure the interlayer space of expandable clays) showed the opposite trend (Figure 8). GLO glauconite yielded the most uniform pathways of K and Fe removal, while the GW8 series showed some incongruent leaching. The GL series displayed the most complicated pathway of leaching.

https://doi.org/10.1346/CCMN.2009.0570503 Published online by Cambridge University Press

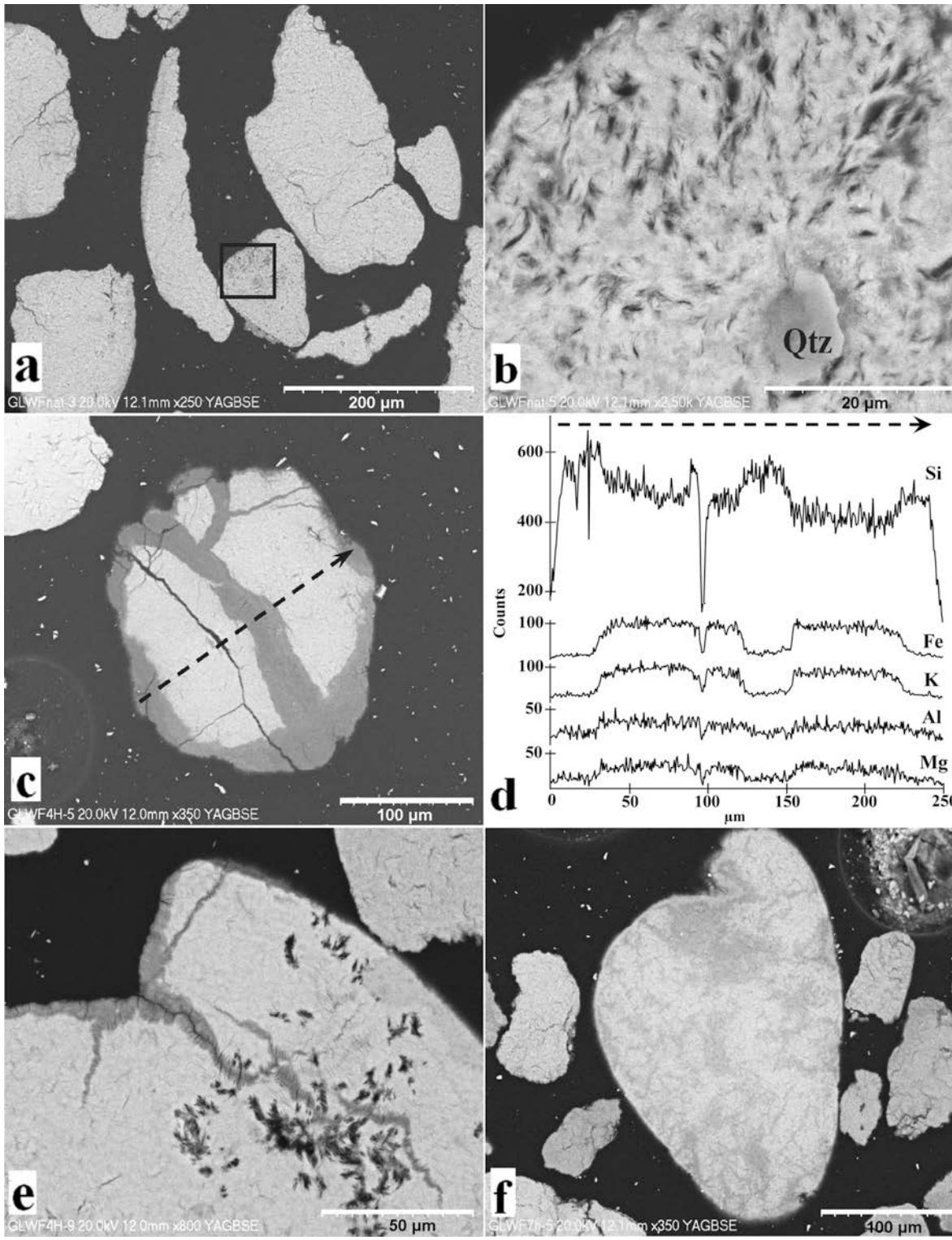

Figure 3. BSE SEM images of the sample GL: (a) GL Nat – shapes of glauconite grains; (b) magnification of the marked area in image a, showing a quartz grain (Qtz) entrapped in glauconite; (c) residual solid GL 4h – image of dissolution pattern (dark-gray area is enriched in silica). The arrow indicates the EDS linescan; (d) Representative EDS linescans of partially dissolved grain from part c (linescans not to scale); (e) residual solid GL 4h – dissolution follows cracks in the grain; (f) residual solid GL 7h – partially dissolved glauconitic grain of a shell shape.

https://doi.org/10.1346/CCMN.2009.0570503 Published online by Cambridge University Press

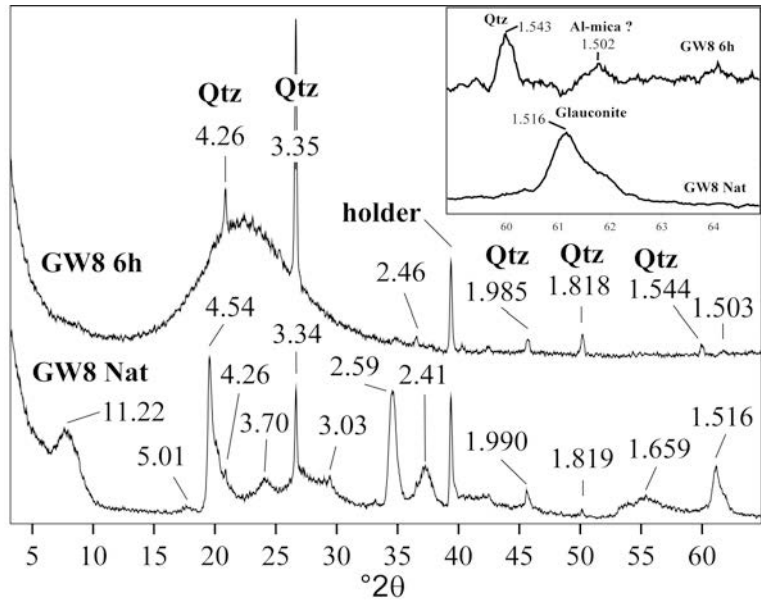

Figure 4. XRD patterns of random preparations of glauconitic grains from the series GW8, natural and after dissolution reaction (6 h). The raised background at the 15–30°2θ range represents amorphous silica. Upper right: zoom of the 060 range, Qtz – quartz.

The FTIR patterns showed evidence of increasing amorphous silica content after increasingly long acid treatments (Figure 9). The characteristic bands of amorphous silica (1090, 800, 467 cm^{-1}; Komadel, 2000) became dominant, while the presence of Fe in the octahedral sheet (817 cm^{-1} – FeFeOH bending; ~680 cm^{-1} – Fe-O out-of-plane; ~500 cm^{-1} – Fe-O-Si bending vibrations: Madejová, 2003; Srasra and Trabelsi-Ayedi, 2000) decreased significantly with time of dissolution. Si-O clay structure vibrations (~1000 cm^{-1} – in-plane stretching Si-O vibrations; 691 cm^{-1} – Si-O out-of-plane vibrations; 447 cm^{-1} – Si-O deformations) also decreased during the acid treatment. The band around 430 cm^{-1}, characteristic of the Si-O-Mg vibration, is undetectable in spite of the presence of Mg in the glauconite structure (Madejová *et*

Table 1. Results of K-Ar dating.

Portion	Proportion (wt.%) of original mass	K_2O (wt.%)	K_2O (% of initial value)	$^{40}Ar^*$ (pmol/g)	% $^{40}Ar^*$	Age (Ma) ±2σ error
GL						
GL Nat	100.0	7.28	100	473.5	75.3	44.6±0.2
GL 1h	94.7	7.57	104.0	403.8	75.5	36.7±0.2
GL 3h	79.3	6.32	86.8	480.6	71.8	52.1±0.2
GL 4h	69.9	4.99	68.5	344.7	33.4	47.4±0.5
GL 7h	64.0	3.47	47.7	550.6	71.3	107.0±0.6
GLO						
GLO Nat	100	7.9 [A]	100	1092.3	90.2	93.6±0.5
GLO Nat	100	7.9 [A]	100	1098.9	88.1	94.1±0.7
GLO Nat	100	7.9 [A]	100	1121.0	87.4	96.0±0.5
GLO 1h	74.7	5.31	67.2	772.1	58.4	98.3±1.7
GW8						
GW8 Nat	100	6.25	100	1171.3	91.4	125.7±0.7
GW8 0.5h	80.6	4.93	78.9	976.5	73.7	132.6±0.9
GW8 1h	61.0	1.84	29.4	448.6	50.9	161.9±2.1
GW8 3h	54.5	0.53	8.5	238.8	27.1	288.7±6.4
GW8 4h	53.5	0.29	4.6	184.2	19.0	394.7±15.3

[A] default average value measured for the GLO standard.
% $^{40}Ar^*$ - fraction of $^{40}Ar^*$ in the total measured ^{40}Ar

https://doi.org/10.1346/CCMN.2009.0570503 Published online by Cambridge University Press

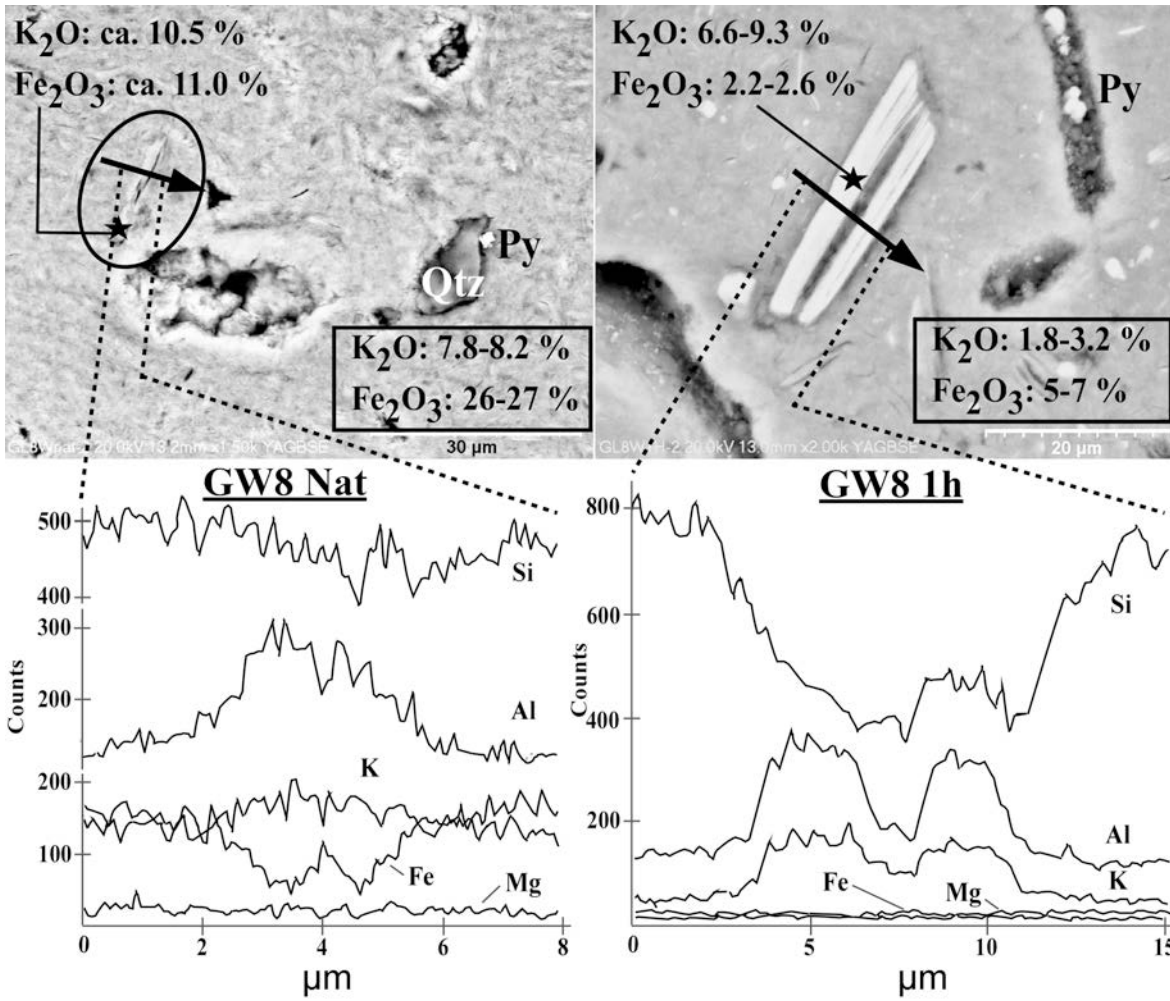

Figure 5. BSE SEM images of the GW8 sample, illustrating minerals entrapped in the glauconite grains. Qtz – quartz, Py – pyrite. The composition of phyllosilicate crystals, enriched in K_2O and depleted in Fe_2O_3 with respect to the glauconite background (values in boxes) was measured in locations marked with asterisks. Arrows mark the EDS linescans presented below the photographs.

al., 1998; Srasra and Trabelsi-Ayedi, 2000). The band at 3547 cm^{-1} is typical of the $MgFe^{3+}OH$ vibrations, while the band at 3570 cm^{-1} comes from OH in the $AlFe^{3+}OH$ group (Besson and Drits, 1997). They both decreased remarkably in the course of the acid treatment. A broad band at 3430 cm^{-1} arose from H-O-H vibrations of adsorbed water. A weak but detectable band at 3613 cm^{-1} may have originated from AlAlOH and AlMgOH pairs (Besson and Drits, 1997).

Isotope dating

K-Ar dating of the GL glauconite (Table 1) revealed clear changes in the ratio of radiogenic argon to potassium ($^{40}Ar^*$ in pmol/g to K_2O in wt.%) in the solid material remaining after dissolution. After 1 h of acid treatment the apparent age decreased from 44.6 to 36.7 Ma. After longer reaction times the apparent age increased to 52.1 Ma (3 h), decreased slightly to 47.4 Ma (4 h), and then increased to 107 Ma (7 h).

The Rb content in the GL series decreased slowly as the dissolution time increased, while the Sr content decreased significantly during 1 h of dissolution, indicating a change in the total Rb/Sr ratio (Table 2). The apparent age can be calculated assuming the formation of glauconite on the seafloor, *i.e.* in equilibrium with the oceanic water (Morton and Long, 1984). Initial $^{87}Sr/^{86}Sr$ values characteristic of Phanerozoic seawater were assumed: 0.707–0.708 for the estimation of apparent ages from the Middle Permian to Middle Oligocene (~260–35 Ma) and 0.708–0.709 for younger dates (see review by Banner, 2004). The general pattern characteristic of K-Ar ages (a decrease and then an increase) is reproduced by the Rb-Sr dates (Table 2), but the changes are much smaller – a nearly three-fold increase for K-Ar, compared to a corresponding 45% increase for Rb-Sr. The <63 µm fraction after 7 h of acid treatment (F 7h) exhibited much older apparent ages: between 182 Ma and 194 Ma. As the solid residue F 7h

https://doi.org/10.1346/CCMN.2009.0570503 Published online by Cambridge University Press

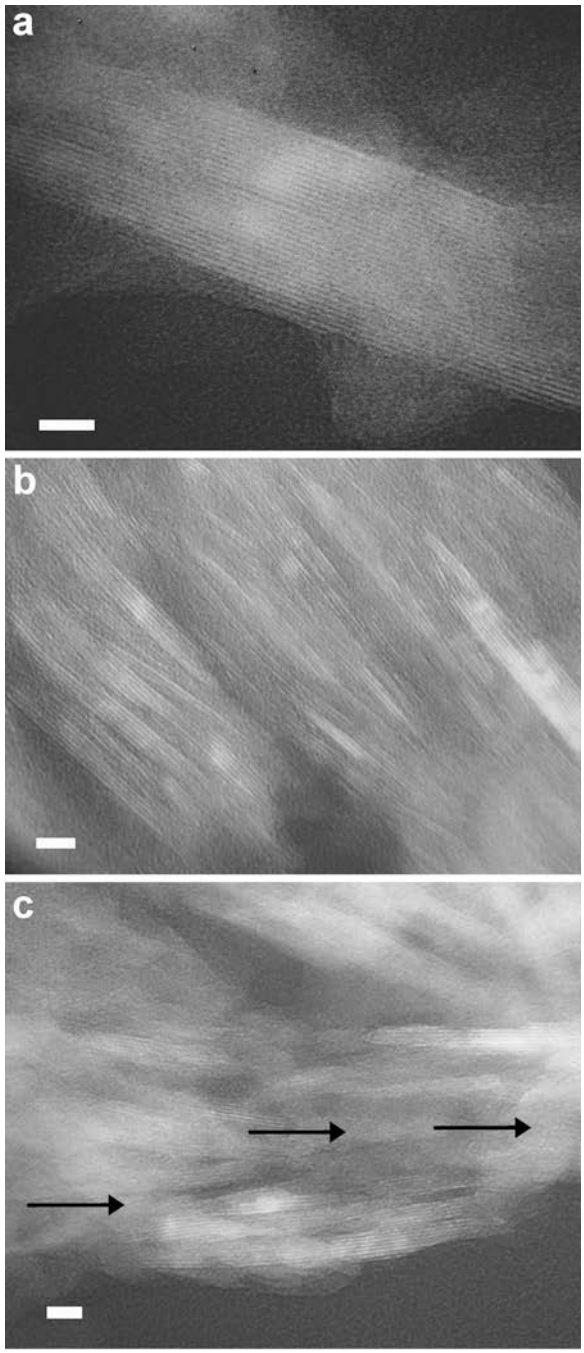

Figure 6. HRTEM images of the GL sample: (a) rare, thick mica particles (>15 layers) were observed in GL Nat (~10 vol.% of all particles); (b) GL 3h, typical glauconite particles from 3 to 7 layers per particle; thick (>15 layers) particles represent <7% of all particles observed. (c) GL 7h showing an increased proportion of amorphous phase (arrows). Scale bar: 10 nm.

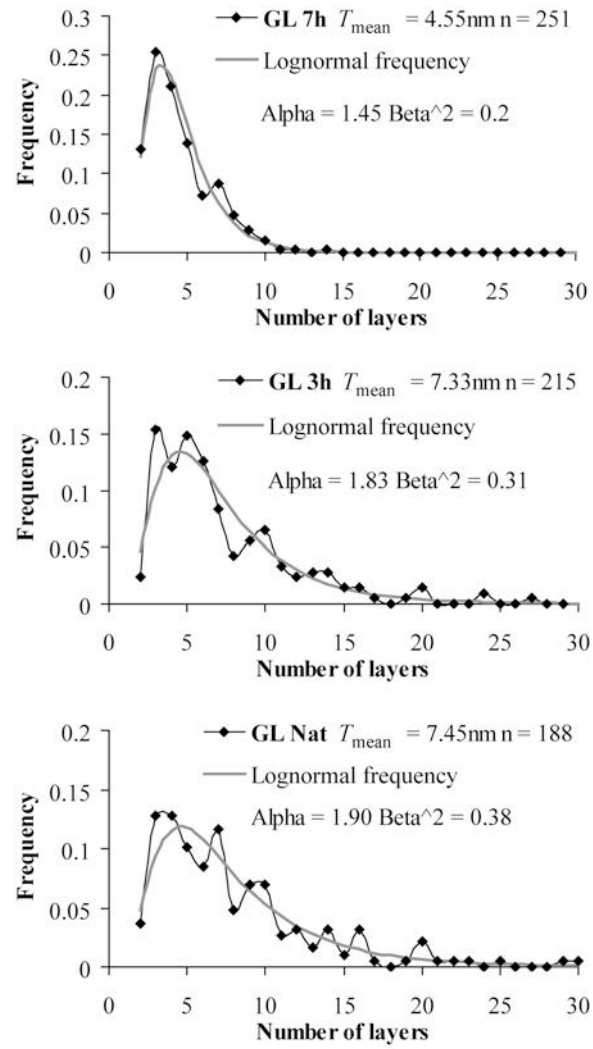

Figure 7. Crystal-thickness distributions and their lognormal fits for the series GL, measured using HRTEM for natural and acid-treated portions. T_{mean} – mean thickness, n – number of measurements, Alpha and Beta^2 – parameters of the lognormal distribution function fitted to the experimental data.

contains much K-bearing material (K-feldspar and Al-rich mica, Figure 2b) of likely non-marine origin, the range of initial $^{87}Sr/^{86}Sr$ values is probably broader than that for the marine sediments. The Rb-Sr isotopic ages were thus calculated using a broader range of initial $^{87}Sr/^{86}Sr$ values (0.705–0.711), considered feasible for non-marine environments. The resulting ages of 205.9 Ma and 170.9 Ma represent possible variability of the apparent age for that mineral mixture.

The apparent ages of the GW8 series increased gradually from 125.7 to 394.7 Ma with increasing times of acid treatment (Table 1). Longer acid treatment also reduced the K content, to 0.29% K_2O. The latter K_2O value is so low that it must be considered to have a large relative error, meaning that the K-Ar apparent age of that sample may be inaccurate.

Multiple K-Ar isotopic ages for the GLO glauconite standard are very close but not identical. They range from 93.6 Ma to 96 Ma, and fall within ~±2% error (std.

https://doi.org/10.1346/CCMN.2009.0570503 Published online by Cambridge University Press

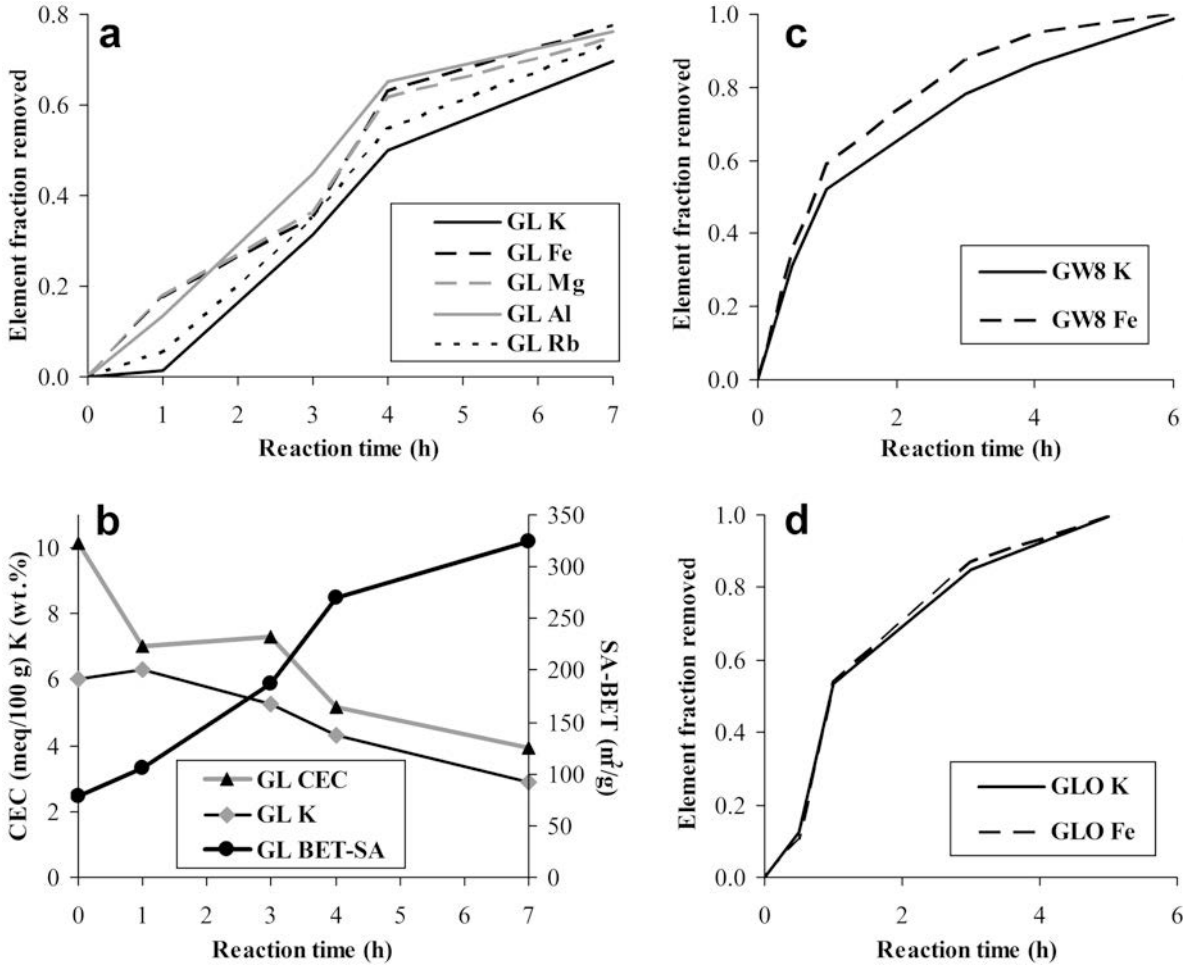

Figure 8. The evolution of interlayer and octahedral cations (a) and changes in CEC, SA-BET values, and K_2O content in the course of dissolution of the GL sample (b), compared to the evolution of K and Fe in the GW8 series (c) and GLO series (d).

dev. = 1.25) confirming a good quality K-Ar measurement. The 1 h treated portion of GLO shows an apparent age of 98.3 Ma, which is insignificantly older than the range of K-Ar ages for the GLO standards.

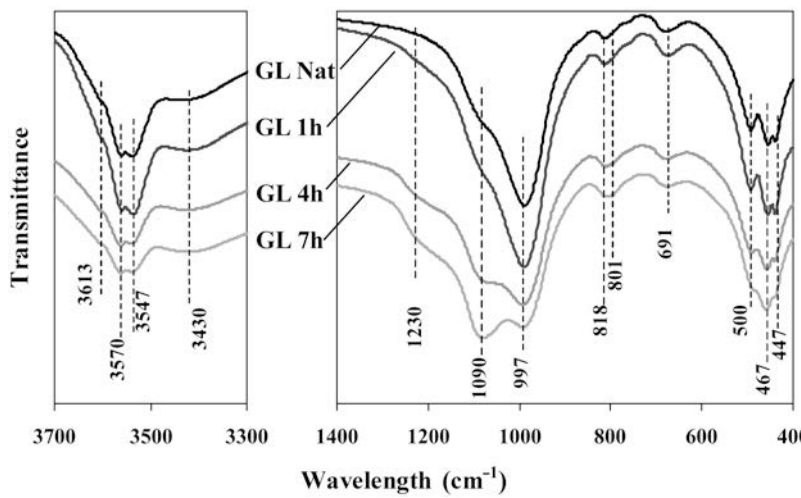

Figure 9. FTIR spectra of the natural and partially dissolved glauconitic grains from the GL sample.

https://doi.org/10.1346/CCMN.2009.0570503 Published online by Cambridge University Press

Table 2. Rb/K and Rb/Sr ratios and Rb-Sr dating results for the GL series with apparent ages calculated using various initial Sr isotopes ratios.

Portion	Rb (ppm)	Rb (% of initial value)	Sr (ppm)	Sr (% of initial value)	Total Rb/Sr	$^{87}Rb/^{86}Sr$	$^{87}Sr/^{86}Sr$	Rb/K ($\times 10^{-4}$)	Initial $^{87}Sr/^{86}Sr$ — Age (Ma) ±2σ error — 0.707	0.708	0.709
GL Nat	261.09	100	31.95	100	8.2	23.69	0.7191	43.20	35.82±0.37	32.85±0.34	29.88±0.32
GL 1h	260.90	94.6	2.66	7.9	98.0	283.94	0.8267	41.52	29.68±0.29	29.43±0.29	29.18±0.29
GL 3h	214.46	65.1	2.35	5.8	91.5	265.04	0.8521	40.88	38.54±0.38	38.27±0.38	38.01±0.37
GL 4h	169.07	45.2	1.92	4.2	88.3	258.68	0.8373	40.82	35.46±0.35	35.19±0.34	34.92±0.34
GL 7h	106.67	26.1	1.25	2.5	85.3	247.32	0.8579	37.03	42.95±0.42	42.67±0.42	42.38±0.42
F 7h	129.07	no data	31.06	no data	4.2	12.04	0.7403	no data	194.3±1.9	188.4±1.9	182.6±1.8

INTERPRETATIONS

Dissolution

Acid treatment of glauconite produces silica residuum. Increasing surface area confirms that the amorphous silica is a microporous material. As demonstrated by Temuujin *et al.* (2003) and Hassan and Baioumy (2006), microporous silica is a product of the solid-state transformation of the tetrahedral sheet. The acid treatment preferentially releases Fe and Mg from the glauconitic grains during the first step of reaction (Figure 8).

The kinetics of Mg and Fe leaching from the GL sample differ from that of K and Al. Potassium persists almost intact during the first hour of treatment, while other elements follow a regular dissolution path. Treatment during subsequent hours led to the release of K, following the same pathway as Al, but shifted towards lower fraction values. Such relations of the leaching curves indicated the presence of at least a two-component system: a high Fe-Mg, low K, easily soluble phase, present in the fresh sample besides the glauconite. Instant dissolution of such a mineral and subsequent slower dissolution of glauconite explain the curves shown in Figure 8a. The CEC evolution during the acid treatment follows strictly the changes in K_2O, excluding the first dissolution step (Figure 8b). The CEC value of the fresh GL sample is much greater than the values that may be predicted from the K_2O curve, indicating the dissolution of a high-CEC phase within the first hour of reaction. All these results suggest the presence of a Mg-Fe-phyllosilicate phase of high CEC, thus vermiculite, nontronite, or high-Fe trioctahedral smectite. Minor (<5%) amounts of such a phase can pass unnoticed by XRD.

The GW8 series shows very different means of K and Fe removal from the GL series. For the first 30 min of acid treatment, both elements are leached in the same fraction while a longer reaction causes removal of 5−10 relative % more Fe than K (Figure 8c). The GLO standard glauconite is considered to be very pure and homogenous and its pathways of K and Fe leaching are almost identical (Figure 8d). Based on the comparison of K and Fe leaching from pure GLO and from differently heterogenous GL and GW8 samples, K and Fe in pure glauconite clearly are removed congruently during acid treatment. This statement remains in agreement with findings by Elliott *et al.* (2002) and probably implies the congruent leaching of all interlayer and octahedral cations of glauconite.

The inhomogenous dissolution of glauconitic samples was observed earlier and explained differently. Studying dissolution of highly expandable glauconite-nontronite, Thompson and Hower (1975) also observed incoherent leaching curves, but with different configuration of the leaching rates. In their interpretation ‘rapidly extracted Fe, Al and Mg is present as interlayer hydroxy-

https://doi.org/10.1346/CCMN.2009.0570503 Published online by Cambridge University Press

complexes in glauconites which show apparent excess octahedral occupancy.' That explanation cannot be applied to almost pure micaceous minerals investigated in this study, because no space exists for the metal-hydroxy complexes in the interlayer. It is contradicted also by a significant reduction in CEC: an increase in CEC would be expected if the hydroxyl interlayers were leached. Srasra and Trabelsi-Ayedi (2000) suggested the dependency of the rates of leaching on the strength of binding between cation and oxygen, as they found the leaching sequence Mg>Fe>Al, which corresponded to the diminishing strength of binding. The present study showed a more complex pathway of leaching.

Dissolution does not proceed as a regular front, attacking grains from the outermost zones. Primary (texture) and secondary (cracks) inhomogeneities in glauconite grains make certain zones more susceptible to acid attack. Besides the quartz grains, micas and pyrite have been found incorporated in the glauconite grains (Figures 3, 5), though only in small amounts, so their influence on the chemical composition of solid residues is negligible. The trace amounts of Al found in almost pure residual silica zones indicate an incomplete transformation of the tetrahedral sheet.

Evolution of K and Rb in the GL material follows the same pathway, as expected from their identical crystallo-chemical positions. But Rb is clearly released in greater amounts than K and the Rb/K ratio of the residual solids decreases over the course of the acid treatment. Such relations imply smaller Rb/K ratios in the detrital phases (enriched in residual solids) compared to the glauconite. A large Sr content in the fresh sample (GL Nat, Table 2) was probably caused by carbonate or phosphate impurities, indicating that the natural GL portion may be so strongly contaminated by Sr of uncertain $^{87}Sr/^{86}Sr$ initial ratio (probably marine, post/syn-depositional), making its Rb-Sr age difficult to determine.

K-Ar dating (detailed calculations given in the Appendix)

A clear tendency was observed for both glauconitic materials (GL and GW8): a general increase of K-Ar apparent age with increasing time of acid treatment, correlated with the decreasing amount of glauconite in the remaining solid. The differential $^{40}Ar^*$ and K_2O values – the virtual concentrations in the material dissolved ($^{40}Ar^*_{(A-B)}$ and $K_2O_{(A-B)}$) – have been calculated using the following equations:

$$^{40}Ar_{(A-B)}{}^{*} = \frac{^{40}Ar_A{}^{*} \times M_A - {}^{40}Ar^*_B \times M_B}{M_A - M_B} \quad (2)$$

and analogous for $K_2O_{(A-B)}$ where $^{40}Ar^*$ is the concentration in a solid portion, M is the mass of the solid portion, and the subscripts A and B indicate the measurement before and after the dissolution step, respectively. Using the standard isotopic age equation and the differential $^{40}Ar^*_{(A-B)}$ and $K_2O_{(A-B)}$ values calculated as above, the differential age (Age_D, in Ma) can be determined:

$$Age_D = Age_{(A-B)} = \frac{1}{\lambda_K} \times \ln\left(\frac{\lambda_K}{\lambda_{K2}} \times \frac{^{40}Ar^*_{(A-B)}}{^{40}K_{(A-B)}} + 1\right) \times 10^{-6} \quad (3)$$

where λ_K and λ_{K2} are constants of the ^{40}K decay (5.543×10^{-10} and 5.81×10^{-11}, respectively). The concentration of ^{40}K is calculated as a fraction of total K. The results of Age_D calculation are listed in Table 3.

Rb-Sr dating (detailed calculations are given in the Appendix)

The Rb-Sr dates of the GL material display a similar trend as observed for its K-Ar data: a decrease followed by an increase (Table 2). The apparent ages calculated upon various assumed initial ratios differ little from each other.

Rb-Sr isotopic ages are usually derived from an isochron, returning also the initial $^{87}Sr/^{86}Sr$ ratio (SI). In the case of glauconite, the SI of the oceanic water of a given geologic period can be assumed, giving the equation:

$$Age = \frac{1}{\lambda_{Rb}} \times \ln\left(\frac{^{87}Sr - {}^{86}Sr \times SI}{^{87}Rb} + 1\right) \times 10^{-6} \quad (4)$$

where $\lambda_{Rb} = 1.42 \times 10^{-11}$, ^{87}Sr, ^{86}Sr, and ^{87}Rb are derived from the data measured during Rb-Sr dating: Rb and Sr concentrations, and $^{87}Rb/^{86}Sr$, $^{87}Sr/^{86}Sr$ ratios, with $^{85}Rb/^{87}Rb = 2.59265$ (Catanzaro *et al.*, 1969).

By analogy to the K-Ar system, the differential age of the dissolved solid can be calculated from the measurements performed before ($_A$) and after ($_B$) (cf. equation 2) the dissolution step:

$$Age_D = Age_{(A-B)} = \frac{1}{\lambda_{Rb}} \times \ln\left(\frac{^{87}Sr_{(A-B)} - {}^{86}Sr_{(A-B)} \times SI}{^{87}Rb_{(A-B)}} + 1\right) \times 10^{-6} \quad (5)$$

where values for $^{87}Sr_{(A-B)}$, $^{86}Sr_{(A-B)}$, and $^{87}Rb_{(A-B)}$ can be calculated in analogous fashion to equation 2.

The differential ages calculated using different initial $^{87}Sr/^{86}Sr$ ratios (Table 4) show a significant variability only for systems involving the natural sample (GL Nat). Such variability is probably a result of the release of non-radiogenic ^{87}Sr from acid-soluble impurities or adsorbed Sr.

Detrital impurities or an artifact?

While the acid treatment reveals mineral impurities (SEM images and XRD patterns), the increase in the K-Ar apparent age of the GL and GW8 samples after acid treatment may reflect the increasing concentrations of the acid-resistant detrital minerals. The contribution

https://doi.org/10.1346/CCMN.2009.0570503 Published online by Cambridge University Press

Table 3. Differential apparent ages (Age_D, Ma) calculated from K_2O and $^{40}Ar^*$ contents (equations 2 and 3 in the text), and masses of partially dissolved glauconitic grains.

Difference between dissolution steps	Mass loss (%)[a]	Mass loss (g)[b]	$K_2O_{(A-B)}$ (wt.%)	$^{40}Ar_{(A-B)}$ (pmol/g)	Age_D (Ma)
GL					
GL Nat – GL 1h	5.3	0.053	2.10	1718.7	494.6
GL Nat – GL 3h	20.7	0.207	10.96	446.2	28.1
GL Nat – GL 4h	30.1	0.301	12.60	772.6	42.1
GL Nat – GL 7h	36.0	0.360	14.05	336.3	16.6
GL 1h – GL 3h	16.3	0.154	14.01	8.3	0.4
GL 1h – GL 4h	26.2	0.248	14.84	570.4	26.5
GL 1h – GL 7h	32.4	0.307	16.12	97.7	4.2
GL 3h – GL 4h	11.9	0.094	16.21	1491.3	62.8
GL 3h – GL 7h	19.3	0.153	18.24	187.6	7.1
GL 4h – GL 7h	8.4	0.059	21.48	−1889.3	n/c
GLO					
GLO Nat – GLO 1h[c]	25.3	0.253	15.55	2063.8	89.9
GW8					
GW8 Nat – GW8 0.5h	19.4	0.194	11.73	1980.6	113.6
GW8 Nat – GW8 1h	39.0	0.390	13.15	2301.7	117.7
GW8 Nat – GW8 3h	45.5	0.455	13.10	2288.2	117.4
GW8 Nat – GW8 4h	46.5	0.465	13.11	2307.1	118.3
GW8 0.5h – GW8 1h	24.3	0.196	14.55	2619.6	121.0
GW8 0.5h – GW8 3h	32.4	0.261	14.12	2516.9	119.8
GW8 0.5h – GW8 4h	33.6	0.271	14.09	2540.8	121.1
GW8 1h – GW8 3h	10.7	0.065	12.82	2207.5	115.8
GW8 1h – GW8 4h	12.3	0.075	12.90	2335.0	121.6
GW8 3h – GW8 4h	1.8	0.010	13.37	3164.4	157.4

[a] Mass loss during a dissolution step calculated as % of the mass before the dissolution step:
Mass loss = $(M_A - M_B)/M_A \times 100\%$ where M_A and M_B are the masses before and after the dissolution step.
[b] Absolute mass loss (g) of 1 g starting material.
[c] Calculated using the middle value (94.1 Ma) of the untreated GLO age.
n/c – not calculated, the calculation would not make any sense.

of the detrital phase to the mixed age would depend on the differences between the crystallization ages and the K_2O contents of the glauconite and the detrital phase.

The GLO glauconite standard can be considered as pure or almost pure homogenous glauconite not containing detrital phases that could affect the isotopic age of the natural GLO. After 1 h of acid treatment, the K concentration in the remaining solid decreased by ~30% compared to the natural glauconite, producing the age of 98.3 Ma. This is not significantly greater than the pure GLO (93.6–96.0 Ma), and can result from a measurement error as well as from a very small amount of a detrital mineral.

Comparing the untreated portions to those subjected to acid treatment, both glauconitic materials (GL and GW8) exhibited an increase in the K-Ar isotopic age, but at different rates. Generally, the rate of the apparent age increase (as % of the initial age *vs.* % of the mass loss) is much greater for GL than for GW8. This greater rate suggests a larger number of detrital component(s) and/or a greater isotopic age difference between the glauconite and the detrital component.

Most differential ages of the GW8 series remain within an acceptable range of the stratigraphic constraints (Lower Hauterivian–Middle Albian), and have values slightly below the K-Ar age of the untreated glauconitic grain. Only the differential ages calculated between the longest dissolution steps are clearly greater, but these values have to be considered as very uncertain due to a large error related to the small mass differences.

The general picture of the differential K-Ar dates of the GL portions is very unclear. Some of the differential isotopic ages are very small, some extremely large, and one differential $^{40}Ar^*$ value is even negative (Table 3). Perhaps no single explanation of that pattern exists. The differential age is very sensitive to laboratory operation errors. Besides the weighting error, material can be lost during acid treatment. Filtration, washing, and the cation exchange procedure might have led to the weight losses.

Very small K or Ar values as well as very small masses imply large errors (*e.g.* differential age between GW8 3h and GW8 4h). Assuming the operator's experience and precision, that part of the error can be minimized by using a sufficiently large mass of starting

https://doi.org/10.1346/CCMN.2009.0570503 Published online by Cambridge University Press

material (>>1 g). The sample must be kept in full suspension during reaction with acid in order to allow all grains to react simultaneously. The glauconitic material cannot be ground before splitting into portions reacted for different periods of time. The weight of splits taken for Ar and K_2O analyses is very small (20–50 mg), so homogeneity of the portions is assumed but may not be perfect. Therefore, a non-uniform distribution of the detrital material in the aggregate of grains is always a question to consider while interpreting extremely small or large differential ages.

Nevertheless, the K-Ar apparent ages increase with acid treatment time for both glauconitic materials, and the Rb-Sr dates, obtained only for the GL sample, confirm the general trend (Figure 10), undoubtedly representing a certain mechanism rather than just a random error. The detrital contamination seems to be the most probable explanation, consistent with the XRD and SEM evidence, and the comparison of K and Fe leaching pathways (Figure 8). For such materials, the smallest differential ages obtained from pairs of portions with high K, Ar, and mass differences (both relative and absolute values) should be considered as closest to the sedimentary age. The K-Ar differential ages for the GL series represent very chaotic and mostly unrealistic values (see the discussion below). The majority of differential ages of the GW8 series meet the requirements specified above and represent a narrow range of ages: from 117.4 Ma to 121.1 Ma (Table 3).

Comparison of K-Ar and Rb-Sr dates for the GL material

Two solid residues of the GL sample fall off the general trend: the decrease in K-Ar and Rb-Sr apparent ages after the first hour of dissolution, and a slight reduction in the isotopic ages for GL 4h. Limited explanations are possible while considering all the observed facts:

(1) An inhomogeneity in the sample aliquots studied.

(2) The decrease in K-Ar and Rb-Sr dates may suggest the presence of a highly-soluble Fe-Mg rich, K-poor phase. If all the mass and CEC decrease after 1 h of treatment is ascribed to this phase, its CEC can be calculated as 60 meq/100 g. A differential age of 495 Ma for the removed phase cannot be trusted because the mass and the K_2O differences are too small (see the discussion above). Weathered biotite/vermiculite is a good candidate to explain these data.

(3) A portion or one of the types of detrital contaminants may have dissolved between the third and fourth hour of the acid treatment, reducing the concentration of the detrital phases in the sample.

Decreases in the Rb/K ratio with reaction time indicated that the detrital, undissolved material contained less Rb than glauconite, a reasonable interpretation, as K-feldspars and Al-micas from pegmatites or metamorphic rocks are strongly depleted in Rb (*e.g.* Stephenson, 2000). The stable rate of decrease in Rb/K is interrupted by the GL 4h portion, yielding a Rb/K ratio very similar to that of the GL 3h portion. This observation correlates with a local decrease in the K-Ar and Rb-Sr apparent ages, an exception from the general trend of increasing apparent ages with the dissolution time (Figure 10).

Isotopic ages measured using K-Ar and Rb-Sr methods for solid residues from the same reactions show the same trend but the absolute values are distinctly different. The increase and variability of Rb-Sr ages is much less than that of K-Ar ages; because the Rb/K ratio of the detrital component is less than that of the glauconite, the influence of the radiogenic ^{87}Sr from the detrital material on the mixed age is less than on the detrital $^{40}Ar^*$.

As mentioned previously, the most reliable differential dates are those represented by pairs of portions representing large differences in K, Ar, Rb, Sr, and mass (both relative and absolute values). While excluding the differential ages based on the GL Nat portion, due to probable occurrence of the easily soluble mineral, the most likely candidates are the pairs GL 1h – GL 4h and

Table 4. Differential apparent Rb-Sr ages (Age_D, Ma) for the GL series, with the calculation based on equations 4 and 5. [a] and [b] are as in Table 3.

Difference between dissolution steps	Mass loss (%)[a]	Mass loss (g)[b]	$^{86}Sr_{(A-B)}$ (ppm)	$^{87}Sr_{(A-B)}$ (ppm)	$^{87}Rb_{(A-B)}$ (ppm)	Initial $^{87}Sr/^{86}Sr$ 0.707	0.708	0.709
						Age_D (Ma)		
GL Nat – GL 1h	5.3	0.053	2.826	2.006	3.903	144.07	93.16	42.21
GL Nat – GL 3h	20.7	0.207	2.890	2.054	25.338	30.76	22.73	14.70
GL Nat – GL 4h	30.1	0.301	2.941	2.100	39.779	36.12	30.92	25.71
GL Nat – GL 7h	36.0	0.360	2.991	2.140	53.672	33.30	29.38	25.45
GL 1h – GL 3h	16.3	0.154	0.064	0.048	21.435	10.11	9.90	9.69
GL 1h – GL 4h	26.2	0.248	0.115	0.094	35.8760	24.37	24.14	23.92
GL 1h – GL 7h	32.4	0.307	0.165	0.134	49.769	24.61	24.37	24.14
GL 3h – GL 4h	11.9	0.094	0.051	0.046	14.4412	45.53	45.28	45.03
GL 3h – GL 7h	19.3	0.153	0.1018	0.0863	28.3343	35.57	35.32	35.07
GL 4h – GL 7h	8.4	0.059	0.0503	0.0406	13.8931	25.22	24.97	24.71

https://doi.org/10.1346/CCMN.2009.0570503 Published online by Cambridge University Press

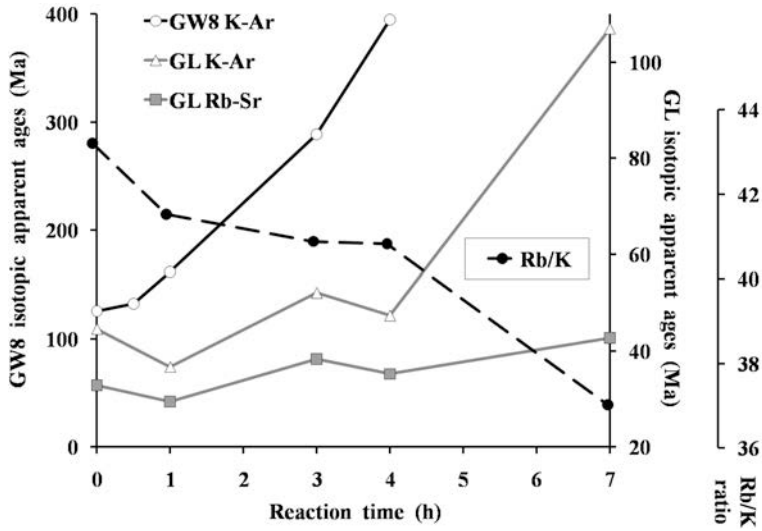

Figure 10. Evolution of the apparent isotopic ages and the Rb/K ($\times 10^{-4}$) ratio with increasing time of acid treatment. All Rb-Sr ages shown were calculated using the initial $^{87}Sr/^{86}Sr$ ratio of 0.708.

GL 1h – GL 7h. Rejecting the age 4.2 Ma as unrealistic, the other ages are 24 Ma (Rb-Sr age) and 26.5 Ma (K-Ar age).

The solid residue F 7h can be used as the reference for the detrital phases in the glauconitic material. The Rb-Sr apparent age estimated for this material varies between 170.9 Ma and 205.9 Ma if the initial $^{87}Sr/^{86}Sr$ values used were broad, to cover the non-sedimentary origin of the detrital minerals. F 7h represents a mixture of the sedimentary glauconite (<40 Ma old) and the detrital components, so the average isotopic age of the detrital minerals must be >200 Ma and there is no reason to believe that the detrital material in the <63 μm fraction is very different from the detrital phases in the glauconitic grains.

Probabilistic models

With so many variables, possible ranges, and assumptions, calculation of the content, composition, and isotopic age of the detrital components is difficult, so probabilistic modeling was employed.

In the model input for the series GL (Table 5), the portion GL Nat was rejected from the series chosen for modeling as it fails to meet the model requirements. The occurrence of the easily soluble old phase and the Rb and K_2O concentrations probably being much different from the acid-resistant detrital mineral would disrupt the calculations. Although the model is not perfect, the trend of variability of the modeled K-Ar and Rb-Sr isotopic ages and the evolution of modeled Rb and K_2O concentrations are very consistent with the measured values. The isotopic ages and K_2O and Rb concentrations calculated for authigenic and detrital minerals remain in agreement with other results and stratigraphic constraints: the computed age of crystallization of glauconite is 32.3 Ma (24 Ma and 26.5 Ma selected from the differential ages), while the computed average isotopic age of the K-bearing detrital mineral is 525.8 Ma. The latter apparent age probably represents the average of the detrital mixture of K-feldspar and Al-rich micaceous mineral.

While the Rb-Sr dating was not applied for the series GW8 (Table 6), the optimization model yields a greater degree of freedom (14 unknowns, 10 equations) than for the GL series. The smaller number of constraints (no Rb-Sr, although one more portion was used) and greater accuracy in sample preparation and handling than for the series GL provided an extremely small total error and a perfect fit. The optimization for GL8 could not give a unique solution; therefore, the most restrictive constraints had to be used (*e.g.* the range of probable sedimentary ages was taken from the differential equations, Table 3). The probabilistic model for the GW8 series, involving Fe, however, did not return a feasible solution. The Fe evolution may be affected by pyrite and, therefore, the equations given (see Appendix) are invalid. Various tested models, based on K_2O content and the K-Ar dates, resulted in the isotopic ages for glauconite remaining within the range 117.3–121.8 Ma, and for the detrital mineral within 401.3–409.7 Ma (generally K_2O >7 wt.%).

The tests conducted with the probabilistic models revealed that the results are very sensitive to changes in model constraints, scaling factors, and the starting values of the optimization procedure. While the model for the GL series did not provide a feasible solution (modeled sedimentary age greater than the measured age), the fit for the GW8 series is very good, probably because of the small number of constraints. The attempt to use probabilistic models for the evaluation of the isotope data is promising but not conclusive, and further testing of this approach is needed.

https://doi.org/10.1346/CCMN.2009.0570503 Published online by Cambridge University Press

Table 5. The applied restrictions and the calculated results for the variables of the series GL introduced into the mathematical optimization model.

Variable	Model variable	MIN value	MAX value	Calculated value
Parameters of components				
Authigenic glauconite	Rb (ppm)	260.0	300.0	263.5
	K_2O (wt.%)	7.00	7.80	7.58
	Isotopic age	10.0	40.0	32.3
Detrital mineral	Rb (ppm)	10.0	200.0	28.1
	K_2O (wt.%)	2.00	13.00	5.45
	Isotopic age	170.0	1000.0	525.8
Sample composition				
GL 1h	Glauconite content (wt.%)	95.0 [A]	99.9 [A]	98.9
	Inactive component content (wt.%)	0.1	10.0	0.1 (limit)
	K-Ar apparent age (Ma)	measured 36.7±0.2		36.3
	Rb-Sr apparent age (Ma)	measured 29.43±0.5		32.8
	K_2O (wt.%)	measured 7.57±0.2		7.55
	Rb (ppm)	measured 260.9±2.6		260.9
GL 3h	Glauconite content (wt.%)	80.0 [A]	99.9 [A]	80.9
	Inactive component content (wt.%)	5.0	40.0	14.9
	K-Ar apparent age (Ma)	measured 52.1±0.2		52.4
	Rb-Sr apparent age (Ma)	measured 38.27±0.65		35.0
	K_2O (wt.%)	measured 6.32±0.2		6.36
	Rb (ppm)	measured 214.5±2.1		214.3
GL 4h	Glauconite content (wt.%)	80.0 [A]	99.9 [A]	63.9
	Inactive component content (wt.%)	5.0	50.0	33.6
	K-Ar apparent age (Ma)	measured 47.4±0.5		47.6
	Rb-Sr apparent age (Ma)	measured 35.2±0.62		34.3
	K_2O (wt.%)	measured 4.99±0.2		4.98
	Rb (ppm)	measured 169.1±1.7		169.1
GL 7h	Glauconite content (wt.%)	60.0 [A]	98.0 [A]	39.6
	Inactive component content (wt.%)	40.0	70.0	51.9
	K-Ar apparent age (Ma)	measured 107.0±0.6		106.9
	Rb-Sr apparent age (Ma)	measured 42.6±0.72		43.4
	K_2O (wt.%)	measured 3.47±0.15		3.46
	Rb (ppm)	measured 106.7±1.1		106.7

[A] MIN and MAX values before normalization on the silica content, where %GLAUC + %DET = 100

CONCLUSIONS

The sequential acid dissolution of glauconite can reveal the presence of detrital impurities and help to estimate the accuracy of dating. Even apparently K-Ar datable, mature glauconite (*sensu* Odin and Matter, 1981) may contain undetectable K-bearing detrital components, which can significantly increase the apparent age of glauconite. All samples used for K-Ar dating must undergo cation exchange to remove exchangeable K^+ cations from the exchange sites. The K^+adsorbed can act in an opposite fashion to the detrital impurities – by decreasing the K-Ar isotopic age of the material studied.

The concept of acid treatment of phyllosilicates works well only for phases with different Fe and Mg contents. Such a limitation is not crucial for glauconite as the most common K-bearing detrital contaminants are trioctahedral micas (instantly soluble) or Al-rich dioctahedral micas and K-feldspar (much more acid-resistant than glauconite). The conditions of reaction must be chosen properly to dissolve a sample sequentially (Yadav *et al.*, 2000). Acid treatments carried out by Morton and Long (1980) and Clauer *et al.* (1993) did not show significant changes in age, due to too the mild conditions of the reaction (room temperature, short time, low acid concentration), even if the samples did contain detrital impurities.

The Rb-Sr system may be less susceptible than K-Ar to the error related to old impurities, if the Rb/K ratio is significantly smaller for the detrital components than for the authigenic glauconite. However, the Rb-Sr system does not offer results in the form of a single age. The initial $^{87}Sr/^{86}Sr$ ratio must be assumed to be the oceanic water ratio and estimated based on a feasible range of ages. The initial $^{87}Sr/^{86}Sr$ ratio of the detrital components remains unknown, increasing the uncertainty in the Rb-Sr dating.

Regardless of the dating system used, if differential dating is applied, special attention must be paid to the

https://doi.org/10.1346/CCMN.2009.0570503 Published online by Cambridge University Press

Table 6. The applied restrictions and an example of the calculated results for the variables of the GW8 series introduced into the mathematical optimization model. [A] – see Table 5.

Variable	Model variable	MIN value	MAX value	Calculated value
Parameters of components				
Authigenic mineral	K_2O (wt.%)	5.5	8.0	6.29–6.36
	Isotopic age	113.0	122.0	117.3–121.8
Detrital mineral	K_2O (wt.%)	6.0	12.0	7.29–11.09
	Isotopic age	380.0	700.0	401.3–409.7
Sample composition (example)				
GW8 Nat	Glauconite content (wt.%)	20.0 [A]	99.9 [A]	96.1
	Inactive component content (wt.%)	0.1	3.0	2.7
	K-Ar apparent age (Ma)	measured 125.7±0.7		125.7
	K_2O (wt.%)	measured 6.25±0.2		6.25
GW8 0.5h	Glauconite content (wt.%)	20.0 [A]	99.9 [A]	74.0
	Inactive component content (wt.%)	5.0	40.0	24.0
	K-Ar apparent age (Ma)	measured 132.6±0.9		132.6
	K_2O (wt.%)	measured 4.93±0.2		4.93
GW8 1h	Glauconite content (wt.%)	5.0 [A]	99.9 [A]	24.9
	Inactive component content (wt.%)	5.0	90.0	72.8
	K-Ar apparent age (Ma)	measured 161.9±2.1		161.9
	K_2O (wt.%)	measured 1.84±0.15		1.84
GW8 3h	Glauconite content (wt.%)	1.0 [A]	98.0 [A]	3.5
	Inactive component content (wt.%)	5.0	98.0	93.7
	K-Ar apparent age (Ma)	measured 288.7±6.4		288.7
	K_2O (wt.%)	measured 0.53±0.1		0.53
GW8 4h	Glauconite content (wt.%)	0.5 [A]	98.0 [A]	0.1
	Inactive component content (wt.%)	5.0	98.0	97.3
	K-Ar apparent age (Ma)	measured 394.7±15.3		394.7
	K_2O (wt.%)	measured 0.29±0.1		0.29

mass balance and accuracy of the measurement. The potential sources of error include: (1) the loss of mass during laboratory procedures; (2) the inhomogeneity of the portions used; and (3) the weighing error. The differential dating based on reactions of large sample quantities leading to large mass differences seem to be the most reliable. The series GL was the pilot experiment, and was handled with less care than is now recommended as a result of this study. The probabilistic modeling, therefore, gave a worse fit for GL than for the series GW8, and the differential ages for GL are also less reliable. For the glauconitic material from the Lublin area (sample GL), it is difficult to decide which isotopic date is the closest to the true crystallization age: 24.0 and 26.5 Ma, calculated from the differential age equations (Rb-Sr and K-Ar, respectively), or the age computed from the probabilistic model (32.3 Ma). All these values remain in agreement with the stratigraphic constraints. The material had been classified as evolved and apparently datable, but showed a K-Ar age of 44.6 Ma – greater than the stratigraphic age. The GW8 material – appearing too poor in K_2O to be datable – showed a very good consistency of the apparent age calculated from the differential age equations and the probabilistic modeling: 119.3 Ma. This age seems very probable for the stratigraphic age. The detrital impurity turned out to be almost negligible for the dating of the untreated GW8 material. The standard GLO glauconite was verified as essentially impurity-free datable glauconite.

The proposed methods based on partial dissolution, applying probabilistic models, and differential age calculations allow evaluation of the reliability of glauconite dating.

ACKNOWLEDGMENTS

The authors thank Jana Madejová and the reviewers, Marion Wampler, W. Burleigh Harris, and Crawford Elliott, for many helpful suggestions. Mrs Dorota Bakowska is acknowledged for her work in the laboratory. The authors are also grateful to Stephan Hlohowskyj for his work on the English. The present study was supported financially by the Polish Ministry of Education and Science, grant no. 2 P04D 034 28, by the Slovak Grant Agency VEGA (project no. 1/3071/06), and by the internal project no 2.5/2005 of the Institute of Geological Sciences, Polish Academy of Sciences.

REFERENCES

Amorosi, A. (1997) Detecting compositional, spatial, and temporal attributes of glaucony: a tool of provenance research. *Sedimentary Geology*, **109**, 135–153.

Aronson, J.L. and Douthitt, C.B. (1986) K/Ar systematics of an acid-treated illite/smectite: implications for evaluating age and crystal structure. *Clays and Clay Minerals*, **34**, 473–482.

Bachliński, R. and Smulikowski, W. (2002) Preliminary Rb-Sr isotope study of the Karkonosze-Kowary gneisses and related rocks. *Mineralogical Society of Poland, Special Papers*, **20**, 53–56.

Banner, J.L. (2004) Radiogenic isotopes: systematics and applications to earth surface processes and chemical stratigraphy. *Earth-Science Reviews*, **65**, 141–194.

Besson, G. and Drits, V.A. (1997) Refined relationships between chemical composition of dioctahedral fine-grained mica minerals and their infrared spectra within the OH stretching region. Part I: identification of the stretching bonds. *Clays and Clay Minerals*, **45**, 158–169.

Bonhomme, M.R., Thuizat, R., Pinault, Y., Clauer, N., Wendling, R., and Winkler, R. (1975) Méthode de datation potassium-argon. Appareillage et technique. *Note technique Inst. Géol. Univ. Strasbourg*, **3**, 53 pp.

Brindley, G.W. and Brown, G. (1980) *Crystal Structures of Clay Minerals and their X-ray Identification.* Monograph No. **5**, Mineralogical Society, London.

Brookins, D.G., Register Jr., J.K., and Krueger, H.W. (1980) Potassium-argon dating of polyhalite in southeastern New Mexico. *Geochimica et Cosmochimica Acta*, **44**, 635–637.

Catanzaro, E.J., Murphy, T.J., Garner, E.L., and Shields, W.R. (1969) Absolute isotopic abundance ratio and atomic weight of terrestrial rubidium. *Journal of Research of the U.S. National Bureau of Standards*, **73A**, 511–516.

Chaudhuri, S., Środoń, J., and Clauer, N. (1999) K-Ar dating of the illitic fractions of Estonian "blue clay" treated with alkylammonium cations. *Clays and Clay Minerals*, **47**, 96–102.

Clauer N., Chaudhuri S., Kralik M., and Bonnot-Courtois Ch. (1993) Effects of experimental leaching on Rb-Sr and K-Ar isotopic systems and REE contents of diagenetic illite. *Chemical Geology*, **103**, 1–16.

Dudek, T., Środoń, J., Eberl, D.D., Elsass, F., and Uhlík, P. (2002) Thickness distribution of illite crystals in shales. I: X-ray diffraction vs. High-resolution transmission electron microscopy measurements. *Clays and Clay Minerals*, **50**, 562–577.

Elliott, W.C., Wampler, J.M., and Elser, A.M. (2002) Clues to the chemical character of the Twiggs Clay glaucony from X-ray diffraction and chemical extractions. *39th Annual Meeting of the Clay Minerals Society, Abstracts with Program*, p. 74.

Espantaleón, A.G., Nieto, J.A., Fernández, M., and Marsal, A. (2003) Use of activated clays in the removal of dyes and surfactants from tannery waste waters. *Applied Clay Science*, **24**, 105–110.

Evernden, J.F., Curtis, G.H., Obradovich, J., and Kistler, R. (1961) On the evaluation of glauconite and illite for dating sedimentary rocks by the potassium-argon method. *Geochimica et Cosmochimica Acta*, **23**, 78–99.

Gazda, L. and Karaś, S. (2002) Trzeciorzędowe piaski kwarcowe Niziny Lubartowskiej (Tertiary quartz sands from the Lubartów Lowland; in Polish). *Scientific papers of the Institute of Mining, Polytechnic of Wrocław*, **97**, 81–188.

Gradstein, F.M., Ogg, J.G., and Smith, A.G. (2004) *A Geologic Time Scale 200*4. Cambridge University Press, Cambridge, UK.

Gregg, S.J. and Sing, K.S.W. (1982) *Adsorption, Surface Area and Porosity*. 2nd edition. Academic Press, London.

Hassan, M.S. and Baioumy, H.M. (2006) Structural and chemical alteration of glauconite under progressive acid treatment. *Clays and Clay Minerals*, **54**, 491–499.

Jackson, M.L. (1969) *Soil Chemical Analysis – Advanced Course*. 2nd edition. Published by the author, University of Wisconsin, Madison, USA.

Józefaciuk, G. and Bowanko, G. (2002) Effect of acid and alkali treatments on surface areas and adsorption energies of selected minerals. *Clays and Clay Minerals*, **50**, 771–783.

Kaim, A. (2002) Gradual evolution of the Early Cretaceous marine gastropod *Rissoina lineage* in central Poland. *Acta Palaeontologica Polonica*, **47**, 667–672.

Kalinowski, B.E. and Schweda, P. (1996) Kinetics of muscovite, phlogopite, and biotite dissolution and alteration at pH 1–4 at room temperature. *Geochimica et Cosmochimica Acta*, **60**, 367–385.

Kelley, S. (2002) Excess argon in K-Ar and Ar-Ar geochronology. *Chemical Geology*, **188**, 1–22.

Komadel, P. (2000) Chemically modified smectites. *Clay Minerals*, **38**, 127–138.

Łącka, B., Giresse, P., Wesołowska, T., and Kubiatowicz-van der Baan, W. (1989) Diagenesis of Neocomian marine fine-grained sediments from Tomaszów Syncline (Central Poland). *Mineralogical Archives*, **43**, 17–39.

Łozińska-Stępień, H., Rytel, A., and Saliński, P. (1985) *Objaśnienia do szczegółowej mapy geologicznej Polski. Arkusz Lubartów. (Explanations of the detailed geological map of Poland – Lubartów Area.)* Wydawnictwa Geologiczne, Warszawa.

Madejová, J. (2003) FTIR techniques in clay mineral studies. *Vibrational Spectroscopy*, **31**, 1–10.

Madejová, J., Bujdák, J., Janek, M., and Komadel, P. (1998) Comparative FT-IR study of structural modifications during acid treatment of dioctahedral smectites and hectorite. *Spectrochimica Acta A*, **54**, 1397–1406.

Manghnani, M.H. and Hower, J. (1964) Glauconites: cation exchange capacities and infrared spectra. Part I. The cation exchange capacity of glauconite. *American Mineralogist*, **49**, 586–598.

Marcinowski, R. and Rudowski, S. (1980) Biała Góra II – kopalnia piasków szklarskich – alb środkowy i górny (in Polish). Pp. 221–226 in: *Przew. 52 Zjazdu PTG, Bełchatów* (W. Barczyk, editor). Wydawnictwa Geologiczne, Warszawa.

Morton, J.P. and Long, L.E. (1980) Rb-Sr dating of Paleozoic glauconite from the Llano region, central Texas. *Geochimica et Cosmochimica Acta*, **44**, 663–672.

Morton, J.P. and Long, L.E. (1984) Rb-Sr ages of glauconite recrystallization: dating times of regional emergence above sea level. *Journal of Sedimentary Petrology*, **54**, 495–506.

Novák, I. and Číčel, B. (1978) Dissolution of smectites in hydrochloric acid: II. Dissolution rate as a function of crystallochemical composition. *Clays and Clay Minerals*, **25**, 341–344.

Odin, G.S. (1969) Méthode de separation des grains de glauconie intérêt de leur étude morphologique et structurale. *Revue de Géologie Dynamique et de Géographie Physique*, **XI**, **2**, 171–176.

Odin, G.S. (1982) How to measure glaucony ages. Pp. 387–403 in: *Numerical Dating in Stratigraphy* (G.S. Odin, editor). John Wiley & Sons, Chichester, UK.

Odin, G.S. (1988) Glaucony from the Gulf of Guinea. Pp. 225–249 in: *Green Marine Clays* (G.S. Odin, editor). Elsevier, Amsterdam.

Odin, G.S. and Dodson, M.H. (1982) Zero isotopic age of glauconites. Pp. 277–305 in: *Numerical Dating in Stratigraphy* (G.S. Odin, editor). John Wiley & Sons, Chichester, UK.

Odin, G.S. and Matter, A. (1981) De glauconiarum origine. *Sedimentology*, **28**, 611–641.

Olsen, J.C. (1910) *A Textbook of Quantitative Chemical Analysis*. 4th Edition. D. van Nostrand Co., New York. p. 189.

Orsini, L. and Remy, J.C. (1976) Utilisation du chlorure de cobaltihexammine pour la détermination simultanée de la capacité d'échange et des bases échangeables des sols.

Science du Sol, **4**, 269–275.
Sandler, A., Harlavan, Y., and Steinitz, G. (2004) Early formation of K-feldspar in shallow-marine sediments at near-surface temperatures (southern Israel): evidence from K-Ar dating. *Sedimentology*, **51**, 323–338.
Srasra, E. and Trabelsi-Ayedi, M. (2000) Textural properties of acid activated glauconite. *Applied Clay Science*, **17**, 71–84.
Steiger, R.H. and Jäger, E. (1977) Subcommission on geochronology: Convention on the use of decay constants in geo- and cosmochronology. *Earth and Planetary Science Letters*, **36**, 359–362.
Stephenson, N.C.N. (2000) Geochemistry of granulite-facies granitic rocks from Battye Glacier, northern Prince Charles Mountains, East Antarctica. *Australian Journal of Earth Sciences*, **47**, 83–94.
Środoń, J., Eberl, D.D., and Drits, V. (2000) Evolution of fundamental particle-size during illitization of smectite and implications for reaction mechanism. *Clays and Clay Minerals*, **48**, 446–458.
Środoń, J., Drits, V.A., McCarty, D.K., Hsieh, J.C.C., and Eberl D.D. (2001) Quantitative XRD analysis of clay-rich rocks from random preparations. *Clays and Clay Minerals*, **49**, 514–528.
Środoń, J., Clauer, N., Banaś, M., and Wójtowicz, A. (2006) K-Ar evidence for a Mesozoic thermal event superimposed on burial diagenesis of the Upper Silesia Coal Basin. *Clay Minerals*, **41**, 671–692.
Temuujin, J., Okada, K., and MacKenzie, K.J.D. (2003) Preparation of porous silica from vermiculite by selective leaching. *Applied Clay Science*, **22**, 187–195.
Tessier, D. (1984) Etude experimentale de l'organisation des materiaux argileux. Doctoral thesis, University of Paris, 361 pp.
Thompson, G.R. and Hower, J. (1973) An explanation for low radiometric ages from glauconite. *Geochimica et Cosmochimica Acta*, **37**, 1473–1491.
Thompson, G.R. and Hower, J. (1975) The mineralogy of glauconite. *Clays and Clay Minerals*, **23**, 289–300.
Uberna, J. and Odrzywolska-Bieńkowa, E. (1977) Nowe stanowiska osadów górnoeoceńskich na obszarze północnej Lubelszczyzny (in Polish). *Kwartalnik Geologiczny*, **21**, 73–87.
Uhlík, P., Šucha V., Eberl, D.D., Puškelová, L'., and Čaplovičová, M. (2000) Evolution of pyrophyllite particle sizes during dry grinding. *Clay Minerals*, **35**, 423–432.
Witkowski, A. (1967) O gatunku *Endemoceras (Lyticoceras) Noricum (Roem)* z kredy dolnej niecki tomaszowskiej (in Polish). *Kwartalnik Geologiczny*, **11**, 637–647.
Yadav, V.P., Sharma, T., and Saxena, V.K. (2000) Dissolution kinetics of potassium from glauconitic sandstone in acid lixiviant. *International Journal of Mineral Processing*, **60**, 15–36.

(*Received 26 March 2008; revised 16 March 2009; Ms. 0147; A.E. M.A. Velbel*)

APPENDIX

K-AR DATING

The standard radiometric decay equation is:

$$D = D_0 + \mathrm{N} \times [\exp(\lambda \times t) - 1] \quad (1)$$

Where D is the number of atoms of the daughter isotope (^{40}Ar) after time t (Age), D_0 is the initial number of atoms of the daughter isotope (at $t = 0$), N is the number of atoms of the parent isotope (^{40}K) in a sample, and λ is the radioactive isotope decay constant. Once atmospheric ^{40}Ar is removed from the calculation by measuring ^{36}Ar (and applying the appropriate ^{40}Ar/^{36}Ar ratio = 295.5), and no initial ^{40}Ar – except in special cases – is considered, D_0 is assumed to be zero. The pure radiogenic ^{40}Ar, after correcting for the atmospheric ^{40}Ar, is conventionally labeled as ^{40}Ar*. Only ~11% of ^{40}K atoms decay to ^{40}Ar, while 89% decay to ^{40}Ca, so the standard equation 1 for the ^{40}K-^{40}Ar system is:

$$^{40}\mathrm{Ar}^* = \frac{\lambda_{K2}}{\lambda_K} \times {}^{40}\mathrm{K} \times [\exp(\lambda_K \times \mathrm{Age}) - 1] \quad (2)$$

where λ_K is the total decay constant for ^{40}K (5.543×10^{-10}) and λ_{K2} is the decay constant of ^{40}K to ^{40}Ar (5.81×10^{-11}). The values of ^{40}K and ^{40}Ar* are in moles (picomoles, micromoles). In order to obtain the age equation from equation 2:

$$\frac{\lambda_K}{\lambda_{K2}} \times \frac{^{40}\mathrm{Ar}^*}{^{40}\mathrm{K}} + 1 = \exp(\lambda_K \times \mathrm{Age})$$

then

$$\lambda_K \times \mathrm{Age} = \ln\left(\frac{\lambda_K}{\lambda_{K2}} \times \frac{^{40}\mathrm{Ar}^*}{^{40}\mathrm{K}} + 1\right)$$

so, for Age in Ma the equation is:

$$\mathrm{Age} = \frac{1}{\lambda_K} \times \ln\left(\frac{\lambda_K}{\lambda_{K2}} \times \frac{^{40}\mathrm{Ar}^*}{^{40}\mathrm{K}} + 1\right) \times 10^{-6} \quad (3)$$

While ^{40}Ar* is calculated from the ^{40}Ar measured by mass spectrometry, ^{40}K [pmol/g] is calculated from K_2O (%):

$$^{40}\mathrm{K} = \left(\frac{\mathrm{K_2O} \times 0.8301}{100}\right) \times \frac{\left(\frac{^{40}\mathrm{K}}{\mathrm{K}}\right) \times 10^{12}}{MW_K} \quad (4)$$

^{40}K/K = 0.0001167 (fraction of ^{40}K in total K), MW_K = the molecular weight for ^{40}K = 39.964 (the molecular weight for total K = 39.103 can also be used).

The differential ^{40}Ar* and K_2O values – the virtual concentrations in the material dissolved (^{40}Ar*$_{(A\text{-}B)}$ and $K_2O_{(A\text{-}B)}$) – were calculated using the following equations:

$$^{40}\mathrm{Ar}^*_{(A-B)} = \frac{^{40}\mathrm{Ar}^*_A \times M_A - {}^{40}\mathrm{Ar}^*_B \times M_B}{M_A - M_B} \quad (5)$$

and

https://doi.org/10.1346/CCMN.2009.0570503 Published online by Cambridge University Press

$$K_2O_{(A-B)} = \frac{K_2O_A \times M_A - K_2O_B \times M_B}{M_A - M_B} \quad (6)$$

where $^{40}Ar^*$ and K_2O correspond to the concentrations in a solid portion, M – to the mass of the solid portion, and the subscripts A and B indicate the measurement before and after the dissolution step, respectively. Using the differential $^{40}Ar^*_{(A-B)}$ and $K_2O_{(A-B)}$ values calculated above (equations 5 and 6), the differential age (Age_D, in Ma) can be determined:

$$Age_D = Age_{(A-B)} = \frac{1}{\lambda_K} \times \ln\left(\frac{\lambda_K}{\lambda_{K2}} \times \frac{^{40}Ar^*_{(A-B)}}{^{40}K_{(A-B)}} + 1\right) \times 10^{-6} \quad (7)$$

Rb-Sr dating

The standard radiometric decay equation 1 for the Rb-Sr system can be written as follows:

$$^{87}Sr = {}^{87}Sr_{INI} + {}^{87}Rb \times [\exp(\lambda_{Rb} \times Age) - 1] \quad (8)$$

where $^{87}Sr_{INI}$ is the initial concentration of ^{87}Sr for Age = 0 (closing the isotopic system), λ_{Rb} is the decay constant (1.42×10^{-11}). The conventional notification is not the initial ^{87}Sr ($^{87}Sr_{INI}$), but the initial $^{87}Sr/^{86}Sr$ ratio (in this study: SI). Therefore:

$$^{87}Sr_{INI} = {}^{86}Sr \times SI \quad (9)$$

Applying equation 9 to equation 8 and transforming it to obtain the Age:

$$^{87}Sr = {}^{86}Sr \times SI + {}^{87}Rb \times [\exp(\lambda_{Rb} \times Age) - 1]$$

and

$$\frac{^{87}Sr - {}^{86}Sr \times SI}{^{87}Rb} + 1 = \exp(\lambda_{Rb} \times Age)$$

then for Age in Ma:

$$Age = \frac{1}{\lambda_{Rb}} \times \ln\left(\frac{^{87}Sr - {}^{86}Sr \times SI}{^{87}Rb} + 1\right) \times 10^{-6} \quad (10)$$

Total rubidium (Rb_{total}) is formed by two major isotopes, ^{85}Rb and ^{87}Rb, and their ratio is $^{85}Rb/^{87}Rb$ = 2.59265 (Catanzaro *et al.*, 1969). Thus, the concentration of ^{87}Rb is calculated as:

$$\frac{^{87}Rb}{Rb_{total}} + \frac{^{85}Rb}{Rb_{total}} = 1$$

and

$$\frac{^{85}Rb}{^{87}Rb} = 2.59265 \Rightarrow {}^{85}Rb = {}^{87}Rb \times 2.59265$$

Therefore,

$$\frac{^{87}Rb + {}^{87}Rb \times 2.59265}{Rb_{total}} = 1$$

and so,

$$^{87}Rb = \frac{Rb_{total}}{^{85}Rb/^{87}Rb + 1}$$

Since Rb_{total} is determined by chemical analysis in ppm, not moles, to transform ppm into μmol

$$^{87}Rb = \frac{Rb_{total}}{MW_{Rb\times(^{85}Rb/^{87}Rb+1)}} \quad (11)$$

where MW_{Rb} is the molecular weight of total rubidium = 85.47. The values of ^{87}Sr and ^{86}Sr can be derived from the ^{87}Rb concentrations and the ratios $^{87}Rb/^{86}Sr$ and $^{87}Sr/^{86}Sr$:

$$^{86}Sr = \frac{^{87}Rb}{^{87}Rb/^{86}Rb} \quad (12)$$

$$^{87}Sr = {}^{86}Sr \times {}^{87}Sr/^{86}Sr = \frac{^{87}Rb \times {}^{87}Sr/^{86}Sr}{^{87}Rb/^{86}Sr} \quad (13)$$

Using equations 12 and 13 in equation 10:

$$Age = \frac{1}{\lambda_{Rb}} \times \ln\left(\frac{\frac{^{87}Rb\times{}^{87}Sr/^{86}Sr}{^{87}Rb/^{86}Sr} - \frac{^{87}Sr}{^{87}Rb/^{86}Sr} \times SI}{^{87}Rb} + 1\right) \times 10^{-6}$$

then

$$Age = \frac{1}{\lambda_{Rb}} \times \ln\left(\frac{\frac{^{87}Rb\times(^{87}Sr/^{86}Sr-SI)}{^{87}Rb/^{86}Sr}}{^{87}Rb} + 1\right) \times 10^{-6}$$

and, finally

$$Age = \frac{1}{\lambda_{Rb}} \times \ln\left(\frac{^{87}Sr/^{86}Sr - SI)}{^{87}Rb/^{86}Sr} + 1\right) \times 10^{-6} \quad (14)$$

Therefore, the Age equation in the Rb-Sr system can utilize only the isotope ratios $^{87}Rb/^{86}Sr$ and $^{87}Sr/^{86}Sr$, provided conventionally by mass spectrometry analysis.

The differential values of ^{87}Rb, ^{86}Sr, and ^{87}Sr and the differential Rb-Sr isotopic age of the dissolved solid can be calculated from the measurements performed before ($_A$) and after ($_B$) the dissolution step:

$$^{87}Rb_{(A-B)} = \frac{^{87}Rb_A \times M_A - {}^{87}Rb_B \times M_B}{M_A - M_B} \quad (15)$$

https://doi.org/10.1346/CCMN.2009.0570503 Published online by Cambridge University Press

$$^{86}Sr_{(A-B)} = \frac{^{86}Sr_A \times M_A - ^{86}Sr_B \times M_B}{M_A - M_B} \quad (16)$$

$$^{87}Sr_{(A-B)} = \frac{^{87}Sr_A \times M_A - ^{87}Sr_B \times M_B}{M_A - M_B} \quad (17)$$

$$Age_D = Age_{(A-B)} = \frac{1}{\lambda_{Rb}} \times \ln\left(\frac{^{87}Sr_{(A-B)} - ^{86}Sr_{(A-B)} \times SI}{^{87}Rb_{(A-B)}} + 1\right) \times 10^{-6} \quad (18)$$

or

$$Age_D = Age_{(A-B)} = \frac{1}{\lambda_{Rb}} \times \ln\left(\frac{^{87}Sr/^{86}Sr - SI}{(^{87}Rb/^{86}Sr)_{(A-B)}} + 1\right) \times 10^{-6} \quad (19)$$

PROBABILISTIC CALCULATION

Part A

Variables, returned as the result of modeling, and their limits (for the actual values see Tables 5 and 6):

(a) K-Ar and Rb-Sr isotopic age of glauconite (Age_{GLAUC}) and the detrital phase (Age_{DETR}) and, restricted by the pairs of the upper and lower limit, assumed by an operator Age^{MIN}_{GLAUC} - Age^{MAX}_{GLAUC} and Age^{MIN}_{DETR} - Age^{MAX}_{DETR}, respectively.

(b) amount of amorphous silica, quartz, and pyrite (%INACT) – impurities inactive for the K-Ar and Rb-Sr system, but diluting the K, Ar, Rb, and Sr concentrations, with upper and lower limits ($\%INACT^{MIN}$, $\%INACT^{MAX}$).

(c) fraction of glauconite (%GLAUC) in the sum of glauconite and detrital K-bearing minerals (%DETR); where

$$\%GLAUC + \%DETR = 100 \quad (20)$$

and %GLAUC is limited by an operator using $\%GLAUC^{MIN}$ and $\%GLAUC^{MAX}$ values.

(d) K_2O content of glauconite (K_2O_{GLAUC}) and of the detrital mineral (K_2O_{DETR}), limited manually by the upper and lower limits: $K_2O^{MIN}_{GLAUC}$ - $K_2O^{MAX}_{GLAUC}$ and $K_2O^{MIN}_{DETR}$ - $K_2O^{MAX}_{DETR}$, respectively.

(e) Rb concentration in glauconite (Rb_{GLAUC}) and in the detrital mineral (Rb_{DETR}), limited manually by the upper and lower limits: Rb^{MIN}_{GLAUC} - Rb^{MAX}_{GLAUC} and Rb^{MIN}_{DETR} – Rb^{MAX}_{DETR}, respectively.

Part B. Basic calculations

(1) For modeling, the following equations are used for the K-Ar system:

Based on equation 4 and applying the modeled variables K_2O_{GLAUC} and K_2O_{DETR}, the $^{40}K_{GLAUC}$ and $^{40}K_{DETR}$ values are calculated:

$$^{40}K_{GLAUC} = \left(\frac{K_2O_{GLAUC} \times 0.8301}{100}\right) \times \frac{\left(\frac{^{40}K}{K}\right) \times 10^{12}}{MW_K} \quad (21)$$

and

$$^{40}K_{DETR} = \left(\frac{K_2O_{DETR} \times 0.8301}{100}\right) \times \frac{\left(\frac{^{40}K}{K}\right) \times 10^{12}}{MW_K} \quad (22)$$

Utilizing equation 2, the modeled Age_{GLAUC} and Age_{DETR} and values $^{40}K_{GLAUC}$ and $^{40}K_{DETR}$ calculated as above (equations 21 and 22), the $^{40}Ar^*$ values for glauconite ($^{40}Ar^*_{GLAUC}$) and the detrital mineral ($^{40}Ar^*_{DETR}$) can be calculated:

$$^{40}Ar^*_{GLAUC} = \frac{\lambda_{K2}}{\lambda_K} \times ^{40}K_{GLAUC} \times [\exp(\lambda_K \times Age_{GLAUC}) - 1] \quad (23)$$

and

$$^{40}Ar^*_{DETR} = \frac{\lambda_{K2}}{\lambda_K} \times ^{40}K_{DETR} \times [\exp(\lambda_K \times Age_{DETR}) - 1] \quad (24)$$

Then the K_2O and $^{40}Ar^*$ for the mixture of glauconite and the detrital phase are calculated (K_2O_{MIX} and $^{40}Ar^*_{MIX}$), regarding the %GLAUC, %DETR, and %INACT:

$$K_2O_{MIX} = \frac{K_2O_{GLAUC} \times \%GLAUC + K_2O_{DETR} \times \%DETR}{100} \times \left(1 - \frac{\%INACT}{100}\right) \quad (25)$$

$$^{40}Ar^*_{MIX} = \frac{^{40}Ar^*_{GLAUC} \times \%GLAUC + ^{40}Ar^*_{DETR} \times \%DETR}{100} \times \left(1 - \frac{\%INACT}{100}\right) \quad (26)$$

The $^{40}K_{MIX}$ is calculated according to equation 4:

$$^{40}K_{MIX} = \left(\frac{K_2O_{MIX} \times 0.8301}{100}\right) \times \frac{\left(\frac{^{40}K}{K}\right) \times 10^{12}}{MW_K} \quad (27)$$

Following equation 3, the K-Ar isotopic date of the mixture ($Age^{K\text{-}Ar}_{MIX}$) is calculated:

$$Age^{K-Ar}_{MIX} = \frac{1}{\lambda_K} \times \ln\left(\frac{\lambda_K}{\lambda_{K2}} \times \frac{^{40}Ar^*_{MIX}}{^{40}K_{MIX}} + 1\right) \times 10^{-6} \quad (28)$$

https://doi.org/10.1346/CCMN.2009.0570503 Published online by Cambridge University Press

(2) For modeling, the following equations are used for Rb-Sr:

Based on equation 11 and applying the modeled variables Rb_{GLAUC} and Rb_{DETR}, the $^{87}Rb_{GLAUC}$ and $^{87}Rb_{DETR}$ values are calculated:

$$^{87}Rb_{GLAUC} = \frac{Rb_{GLAUC}}{^{85}Rb/^{87}Rb + 1} \quad (29)$$

and

$$^{87}Rb_{DETR} = \frac{Rb_{DETR}}{^{85}Rb/^{87}Rb + 1} \quad (30)$$

Based on equation 1 (for $D_0 = 0$), and using modeled values of Age_{GLAUC} and Age_{DETR}, and calculated $^{87}Rb_{GLAUC}$ and $^{87}Rb_{DETR}$ values (equations 21 and 22), the pure radiogenic $^{87}Sr^*$ values for glauconite ($^{87}Sr^*_{GLAUC}$) and the detrital mineral ($^{87}Sr^*_{DETR}$) are calculated:

$$^{87}Sr^*_{GLAUC} = {}^{87}Rb_{GLAUC} \times [\exp(\lambda_{Rb} \times Age_{GLAUC}) - 1] \quad (31)$$

and

$$^{87}Sr^*_{DETR} = {}^{87}Rb_{DETR} \times [\exp(\lambda_{Rb} \times Age_{DETR}) - 1] \quad (32)$$

Finally, the total Rb and $^{87}Sr^*$ are calculated for the mixture of glauconite and the detrital mineral (Rb_{MIX}, $^{87}Sr^*_{MIX}$, respectively):

$$Rb_{MIX} = \frac{Rb_{GLAUC} \times \%GLAUC + Rb_{DETR} \times \%DETR}{100} \times \left(1 - \frac{\%INACT}{100}\right) \quad (33)$$

$$^{87}Sr_{MIX} = \frac{^{87}Sr_{GLAUC} \times \%GLAUC + {}^{87}Sr_{DETR} \times \%DETR}{100} \times \left(1 - \frac{\%INACT}{100}\right) \quad (34)$$

Analogous to equation 11, the $^{87}Rb_{MIX}$ is calculated

$$^{87}Rb_{MIX} = \frac{Rb_{MIX}}{MW_{Rb} \times (^{85}Rb/^{87}Rb + 1)} \quad (35)$$

Transforming equation 8 or 10 for $^{87}Sr_{INI} = 0$ to calculate the Rb-Sr isotopic date of the mixture ($Age^{Rb\text{-}Sr}_{MIX}$):

$$Age^{Rb-Sr}_{MIX} = \frac{1}{\lambda_{Rb}} \times \ln\left(\frac{^{87}Sr^*_{MIX}}{^{87}Rb_{MIX}} + 1\right) \times 10^{-6} \quad (36)$$

Part C. Optimization

(1) For each portion of the acid-treated glauconite, five measured values are compared with the modeled values (equations 25, 28 and 33, 36): K_2O_{MIX} with measured K_2O (K_2O_{MEAS}), Rb_{MIX} with the measured total Rb (Rb_{MEAS}), $Age^{K\text{-}Ar}_{MIX}$ with the measured K-Ar isotopic date ($Age^{K\text{-}Ar}_{MEAS}$), $Age^{Rb\text{-}Sr}_{MIX}$ with the measured Rb-Sr isotopic age, with SI assumed as 0.7080 for all the values ($Age^{Rb\text{-}Sr}_{MEAS}$), and the Rb/K ratio of the calculated (Rb/K_{MIX}) and measured (Rb/K_{MEAS}) values. The errors (E) between the measured and modeled values were calculated (E_{K_2O}, E_{Rb}, $E_{Age(K\text{-}Ar)}$, $E_{Age(Rb\text{-}Sr)}$, and $E_{Rb/K}$, respectively). Some errors were multiplied by the scaling factors (ScF) of 1, 10, 100, or even 1000, depending on the assumed accuracy of values modeled and their absolute values.

$$E_{K_2O} = (K_2O_{MIX} - K_2O_{MEAS})^2 \times ScF \quad (37)$$

$$E_{Rb} = (Rb_{MIX} - Rb_{MEAS})^2 \times ScF \quad (38)$$

$$E_{Age(K\text{-}Ar)} = (Age^{K\text{-}Ar}_{MIX} - Age^{K\text{-}Ar}_{MEAS})^2 \times ScF \quad (39)$$

$$E_{Age(Rb\text{-}Sr)} = (Age^{Rb\text{-}Sr}_{MIX} - Age^{Rb\text{-}Sr}_{MEAS})^2 \times ScF \quad (40)$$

$$E_{Rb/K} = \left(\frac{Rb_{MIX}}{K_2O_{MIX} \times 0.8301} - \frac{Rb_{MEAS}}{K_2O_{MEAS} \times 0.8301}\right) \times ScF \quad (41)$$

The $E_{Rb/K}$ is a derivative of E_{K_2O} and E_{Rb} but was added as an additional point of fitting.

(2) The total error for each acid-treated portion (E_P) is the sum of the errors. For the GL series, the values of ScF were chosen as follows: for E_{K_2O} ScF = 100, for E_{Rb} ScF = 1, for $E_{Age(K\text{-}Ar)}$ ScF = 100, for $E_{Age(Rb\text{-}Sr)}$, ScF = 100, and for $E_{Rb/K}$ ScF = 1000.

$$E_p = E_{K_2O} + E_{Rb} + E_{Age(K\text{-}Ar)} + E_{Age(Rb\text{-}Sr)} + E_{Rb/K} \quad (42)$$

Four portions of the GL series were fitted simultaneously. The GL Nat portion was rejected from the calculation due to the probability of occurrence of the additional easily soluble phase, which would break the assumption regarding one type (or a mixture with constant ratios of mineral concentrations) of the detrital phase. The E_P value for GL 1h (E_P^{GL1h}), GL 3h (E_P^{GL3h}), GL 4h (E_P^{GL4h}), and GL7h (E_P^{GL7h}) were added to obtain the total error for all portions of the GL series (E^{GL}) used in the modeling:

$$E^{GL} = E_p^{GL1h} + E_p^{GL3h} + E_p^{GL4h} + E_p^{GL7h} \quad (43)$$

(3) The E_P value for the GW8 series was calculated in an analogous way as for GL. Due to the fact that the portions of GW8 were not measured for the Rb concentrations and Rb-Sr isotopic date, E_P is given by the sum:

$$E_p = E_{K_2O} + E_{Age(K\text{-}Ar)} \quad (44)$$

and for E_{K_2O} ScF=1000, while for $E_{Age(K\text{-}Ar)}$ ScF=1.

Five acid-treated portions of the GW8 series were used in the modeling, thus the total error for GW8

https://doi.org/10.1346/CCMN.2009.0570503 Published online by Cambridge University Press

(E^{GW8}) is:

$$E^{GW8} = E_p^{GW\,Nat} + E_p^{GW8\,0.5h} + E_p^{GW8\,1h} + E_p^{GW8\,3h} + E_p^{GW8\,4h} \quad (45)$$

(4) All the variables listed in Part A were modeled during the optimization runs, in order to obtain the smallest possible E^{GL} and E^{GW8} values. Once the Age_{GLAUC} and Age_{DETR}, K_2O_{GLAUC} and K_2O_{DETR}, Rb_{GLAUC} and Rb_{DETR} (the latter two for the GL series only) were the single values modeled for all portions together, *e.g.*:

$$Age_{GLAUC}^{GL\,1h} = Age_{GLAUC}^{GL\,3h} = Age_{GLAUC}^{GL\,4h} = Age_{GLAUC}^{GL\,7h} \quad (46)$$

The %GLAUC, %DETR, and %INACT, and their upper and lower limits, were different for different portions. In such a way the chemistry and isotopic age of the components of the glauconitic pellets (GLAUC, DETR, and INACT) in different stages of the acid dissolution remain the same, while their relative proportions are allowed to change.

The probabilistic mathematical engine – gradient non-linear *Premium Solver Platform*™ 8.0 (Frontline Systems Co.) – added to the model described above is a common method used in various fields. All the details of the optimization strategy were described by Fylstra *et al*. (1998) and Nenov and Fylstra (2003).

REFERENCES

Fylstra, D., Lasdon, L., Watson, J., and Waren, A. (1998) Design and use of the Microsoft Excel Solver. *Interfaces*, **28**, 29–55.

Nenov, I. and Fylstra, D. (2003) Interval methods for accelerated global search in the Microsoft Excel Solver. *Reliable Computing*, **9**, 143–159.

https://doi.org/10.1346/CCMN.2009.0570503 Published online by Cambridge University Press